People’s Democratic Republic of Algeria

Ministry of Higher Education and Scientific Research

University of Echahid Hamma Lakhdar - El Oued

Faculty of Technology

Department of Mechanical Engineering

Dissertation

ACADEMIC MASTER'S

Field: Science and Technology

Department: Mechanical Engineering

Specialization: Energy

Presented by:

1. ABD ELWAHAB GOSSI
2. GHERAIRI FARIS

THÈME

Numerical Analysis and Optimization of Winglet Configurations for Aerodynamic Efficiency Enhancement Using CFD

Dissertation Submitted in Partial Fulfillment of the Requirements for the Master's Electromechanics Degree in Master

Publicly defended in: 14/06/2025

Board of Examiners:

Dr. MOHAMED KHACHANA		Chairman
Dr. KHALIL DEGHOUM		**Superviser**
Dr. DJILANI NASSIB		**Examiner**

Academic Year 2025 – 2026

Acknowledgements

First and foremost, we thank Allah Almighty for granting us the strength and perseverance to complete this work.

We would like to express our sincere gratitude to our supervisor, ***Dr. Khalil Deghoum****, for his valuable guidance, support, and encouragement throughout this project.*

We also extend our thanks to the members of the jury for evaluating this dissertation, and to all our teachers, colleagues, and everyone who contributed directly or indirectly to the completion of this work.

Thank you.

Dedication

To those who bore the responsibility of giving without expecting anything in return,

To those whose prayers were the secret behind my success and an unwavering source of support throughout my journey,

***To my beloved parents**, the source of my strength and inspiration. May God protect them and grant them a long and blessed life.*

To those who shared my moments of fatigue and patience and supported me tirelessly through every challenge,

To my brothers, sisters, and all the members of my dear family.

To my esteemed teachers, who illuminated my path with their knowledge and wisdom,

And to everyone who taught me even a single letter or offered me sincere advice.

To all those who believed in my abilities and contributed, in one way or another, to helping me reach this stage.

I dedicate this humble work as a token of gratitude and appreciation to all those who have contributed to this achievement.

GHERAIRI FARIS

Dedication

First and foremost, I would like to express my deepest gratitude to ***Allah****, who granted me the strength, patience, and determination necessary to accomplish this work. Peace and blessings be upon our Prophet* ***Muhammad (peace be upon him)****.*

I dedicate the fruit of this modest work to ***my beloved parents****, who have always been an endless source of love, support, and sacrifice. Through their encouragement, guidance, and prayers, I have been able to pursue my studies and achieve this goal. May Allah protect them and reward them abundantly.*

To ***my brothers, my sisters, and all my family members****, for their affection, moral support, and constant presence throughout my academic journey.*

To ***my supervisor****, for his availability, valuable advice, scientific guidance, and continuous support, which greatly contributed to the completion of this dissertation.*

To ***all my teachers****, who generously shared their knowledge with dedication and professionalism, and who played an important role in my academic and personal development.*

To ***my friends and colleagues****, with whom I shared moments of hard work, perseverance, and success during my university studies.*

Finally, to everyone who contributed, directly or indirectly, to the accomplishment of this work.

I dedicate this dissertation with the hope that it will represent a modest contribution to the field of ***Energy Engineering*** *and that it may be useful to future researchers and students.*

With all my gratitude and deepest respect.

ABD ELWAHAB GOSSI

Summary

This dissertation examines the aerodynamic performance of the NACA 2412 airfoil using Computational Fluid Dynamics (CFD). It reviews the fundamentals of airfoil theory, including key airfoil families and aerodynamic principles such as lift, drag, pressure coefficient, and Reynolds number. The governing Navier–Stokes equations and the SST k–ω turbulence model are applied for numerical simulation due to their accuracy in turbulent flow prediction. CFD simulations were conducted at different velocities (10, 15, and 20 m/s) and angles of attack (0°, 5°, 10°, and 15°). The results show that increasing the angle of attack increases both lift and drag coefficients, with flow separation occurring at higher angles. Optimal aerodynamic performance is achieved at moderate angles of attack, confirming that CFD is an effective tool for analyzing airfoil behavior.

Keywords: NACA 2412 airfoil, Computational Fluid Dynamics (CFD), aerodynamic performance, lift coefficient, drag coefficient

Résumé

Cette dissertation étudie les performances aérodynamiques du profil NACA 2412 à l'aide de la dynamique des fluides numérique (CFD). Elle présente les bases théoriques des profils aérodynamiques ainsi que les familles principales telles que NACA, Clark Y, RAF, Selig S1223 et NASA, en expliquant les principes fondamentaux comme la portance, la traînée, le coefficient de pression et le nombre de Reynolds. Les équations de Navier–Stokes et le modèle de turbulence SST k–ω sont utilisés pour les simulations en raison de leur précision dans les écoulements turbulents. Les simulations ont été réalisées pour différentes vitesses (10, 15 et 20 m/s) et angles d'attaque (0°, 5°, 10° et 15°). Les résultats montrent une augmentation de la portance et de la traînée avec l'augmentation de l'angle d'attaque, avec apparition de décollement à des angles élevés. Les meilleures performances aérodynamiques sont obtenues à des angles modérés, confirmant l'efficacité de la CFD.

Mots-clés : profil NACA 2412, dynamique des fluides numérique (CFD), performance aérodynamique, coefficient de portance, coefficient de traînée

الملخص

تبحث هذه الأطروحة في الأداء الديناميكي الهوائي لملف الجناح NACA 2412 باستخدام ديناميكا الموائع الحسابية (CFD).تقدم الدراسة مراجعة للأساسيات النظرية للأجنحة الهوائية، بما في ذلك أهم العائلات مثل NACA و Clark Y و RAFو Selig S1223وNASA، إضافة إلى المبادئ الأساسية مثل الرفع، السحب، معامل الضغط، وعدد رينولدز. تم اعتماد معادلات نافير–ستوكس ونموذج الاضطراب SST k–ω لإجراء المحاكاة العددية بدقة عالية. أُجريت المحاكاة عند سرعات مختلفة (10 و15 و20 م/ث) وزوايا هجوم (0°، 5°، 10°، 15°). أظهرت النتائج أن زيادة زاوية الهجوم تؤدي إلى زيادة كل من الرفع والسحب مع حدوث انفصال في الجريان عند الزوايا العالية. وكانت أفضل أداءات ديناميكية هوائية عند الزوايا المتوسطة، مما يؤكد فعالية CFD في تحليل سلوك الأجنحة الهوائية.

الكلمات المفتاحية :الجناح الهوائيNACA 2412 ، ديناميكا الموائع الحسابية(CFD) ، الأداء الديناميكي الهوائي، معامل الرفع، معامل السحب

Contents

Chapter III : Simulation and results

List of Figures

List of Symbols and Abbreviations

Symbol / Acronym	Meaning
α	Angle of Attack
δij	Kronecker Delta
γ	Intermittency Factor
μ	Dynamic Viscosity
μt	Eddy Viscosity
μτ	Friction Velocity
ν	Kinematic Viscosity
ω	Angular Frequency
ρ	Fluid Density
τij	Reynolds Stress Tensor
τ	Stress Tensor
F	Force Vector
g	Gravitational Acceleration
r	Position Vector
V	Velocity Vector
a	Oscillation Amplitude
c	Airfoil Chord Length
Cp	Pressure Coefficient
CD	Drag Coefficient
CL	Lift Coefficient
CT	Thrust Coefficient
D	Drag Force
f	Oscillation Frequency
h	Non-dimensional Amplitude
k	Reduced Frequency
k	Thermal Conductivity

Symbol / Acronym	**Meaning**
L	Characteristic Length
L	Lift Force
l_0	Length Scale
p	Pressure
p_0	Free-stream Pressure
Re	Reynolds Number
Rex,crit	Critical Reynolds Number
T	Oscillation Period
t	Time
t	Maximum Thickness of NACA 00XX Airfoil
U	Characteristic Velocity
u	Velocity Component in x-direction
U_0	Free-stream Velocity
v	Velocity Component in y-direction
v_0	Velocity Scale
x, y	Cartesian Coordinates
BC	Boundary Condition
BL	Boundary Layer
CFD	Computational Fluid Dynamics
CV	Control Volume
DNS	Direct Numerical Simulation
LES	Large Eddy Simulation
LEV	Leading Edge Vortex
MAV	Micro Air Vehicle
RANS	Reynolds-Averaged Navier–Stokes
URANS	Unsteady Reynolds-Averaged Navier–Stokes

General Introduction

General Introduction

Aerodynamics is a fundamental field of fluid mechanics and aerospace engineering that studies the behavior of airflow around bodies, particularly airfoils, which are responsible for generating lift in aircraft. The continuous development of aviation technology has increased the importance of aerodynamic design in improving aircraft performance, reducing fuel consumption, and enhancing flight efficiency.

Airfoil geometry plays a crucial role in determining aerodynamic characteristics such as lift, drag, and stability. Therefore, understanding airflow behavior around airfoils has become essential in modern aircraft design. In this context, Computational Fluid Dynamics (CFD) has emerged as a powerful tool for analyzing aerodynamic phenomena and predicting flow behavior under different operating conditions.

This dissertation investigates the aerodynamic performance of NACA airfoils by studying the effects of angle of attack and flow velocity on pressure and velocity distributions, as well as on lift and drag coefficients. The analysis is based on numerical simulations using the Navier–Stokes equations and the SST k-ω turbulence model.

The results of this study contribute to a better understanding of airfoil aerodynamic behavior and provide useful insights for the design of more efficient and stable aircraft configurations.

Chapter I

Airfoil Fundamentals and Literature Review

I.1 Introduction

Aerodynamics is one of the most important branches of mechanical and aeronautical engineering. It studies the effects of airflow around various objects, particularly airfoils, which are the primary element in generating lift for aircraft. With the continuous development of the aviation industry, airfoil design has become a crucial factor in improving performance, reducing air resistance, and increasing flight efficiency.

This research aims to study airfoils in terms of their operating principle, engineering characteristics, and different types, focusing on the well-known NACA models, which are among the most widely used designs in aviation history. The research also examines the effect of airfoil shape on the dynamic performance of an aircraft and the importance of these designs in the development of modern aeronautical systems.

I.2 Previous studies on Airfoil:

E Nikolaou et al[1] : This study focuses on optimizing the winglet design of a drone using Surrogate-based optimization techniques with CFD. The effects of length, tilt angle, and curvature on performance were analysed. The results showed that using approximate models reduces computation time while maintaining high accuracy. The optimized design also resulted in an increased lift-to-drag ratio (L/D). The study confirmed that winglet optimization enhances the dynamic stability of the aircraft.

Z Lyu et al [2] : This study focuses on optimizing the winglet design of a drone using Surrogate-based optimization techniques with CFD. The effects of length, tilt angle, and curvature on performance were analysed. The results showed that using approximate models reduces computation time while maintaining high accuracy. The optimized design also resulted in an increased lift-to-drag ratio (L/D). The study confirmed that winglet optimization enhances the dynamic stability of the aircraft.

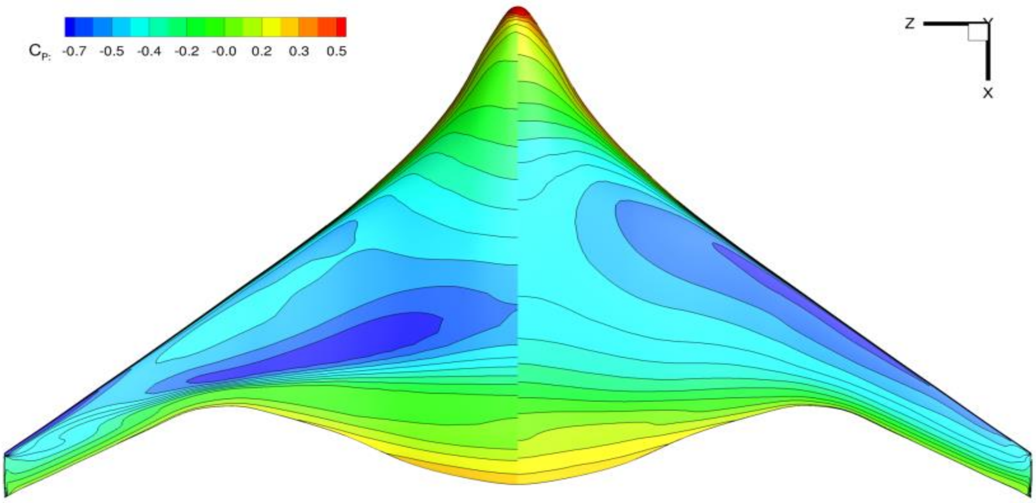

Fig 01: Pressure contour of the baseline and optimized BWB for Case 1 [**2**]

P Panagiotou et al [3] : This paper investigates the impact of design parameters such as the tilt angle (cant) and angle of attack. The results show that a tilt angle of approximately 30° provides optimal performance. The angle of attack also appears to have a lesser impact. The study employed CFD simulation using 3D models. It concludes that selecting the appropriate angles is the crucial factor in improving efficiency.

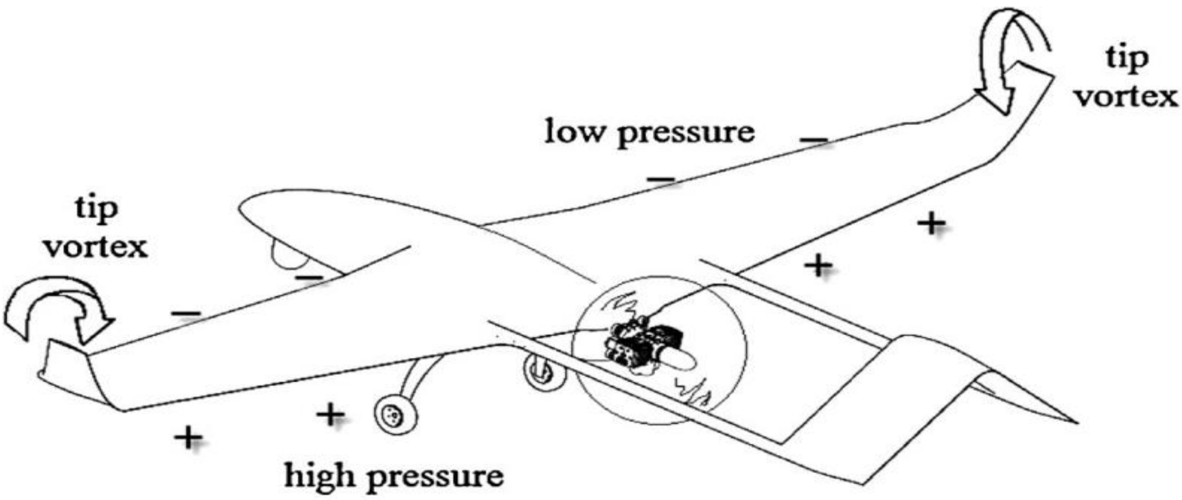

Fig 02: Tip vortex formation [**3**]

A Dela Peña [4] : This study compares passive and active winglets. The results show that active winglets offer better performance under various flight conditions. They also improve fuel efficiency but come with greater structural complexity. High-resolution CFD was used to analyze the performance. The study recommends the use of active winglets in advanced aircraft.

L Lakhdhir [5] : This study focuses on adding winglets to fan blades. The results showed an increase in thrust and efficiency of up to ~9%. However, an increase in energy consumption was also recorded. Furthermore, CFD demonstrated its ability to accurately predict performance (error less than 5%). The study underscores the importance of balancing performance and energy consumption.

S Belfer hat [6]: This study is based on wind tunnel experiments with CFD. Different winglet angles were tested. The results showed that a 55° angle provides the best performance. Lift change with angle of attack was also analyzed. The results confirm the importance of mounting angle in optimizing performance.

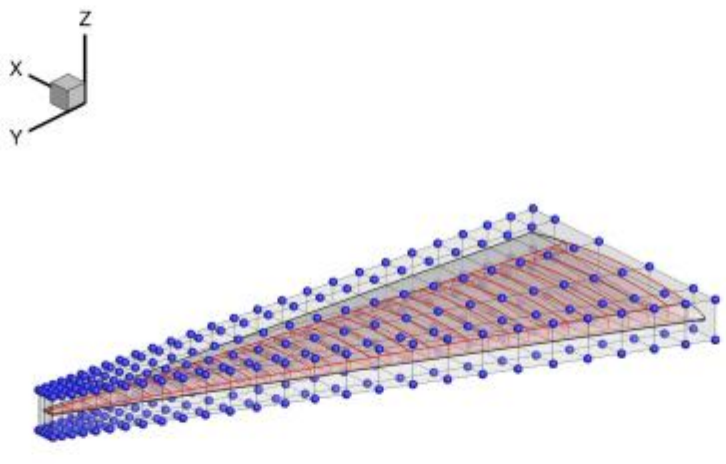

Fig 03: FFD volume around the structural and CFD meshes [**6**]

H Sogukpinar[7] : This study examines the effect of winglets on the L/D ratio using CFD. The results show a significant reduction in induced drag. Pressure distribution across the wing also improves. The effect of different winglet shapes was analyzed. The study concludes that an optimal design significantly increases efficiency.

S Merryisha et al [8] : The focus is on reducing wingtip vortices. The results showed that winglets significantly reduce vorticity intensity, leading to improved aerodynamic efficiency. Flow and pressure lines were analyzed. The study confirms the importance of this technology in modern aviation.

SR Reddy et al[9]: This study utilizes multi-objective optimization (Drag + Lift). Optimization algorithms were employed in conjunction with CFD (Controlled Flow Data). The results demonstrated a balance between performance and efficiency, and fuel consumption was reduced. The study underscores the importance of combining CFD with intelligent algorithms.

HS Helal et all[10]: Dual winglets (split winglets) were studied. The results showed significant improvements compared to traditional designs. Drought was also further reduced. Aerodynamic force distribution was analyzed. The study recommends the use of this type in modern aircraft.

CD Bachmann[11]: The study focused on the Sharklets design used in commercial aircraft. Results showed a significant improvement in fuel consumption. Inductive drag was also reduced. Performance was analyzed at different angles of attack. The study confirms the effectiveness of this design.

AJD Al-Khafaji et all[12] : The study investigates the effect of the angles of inclination and declination. The results show that combining two optimal angles yields the best performance. Optimal values were also determined. The study confirms that the interaction between the parameters is very important**.**

SAS Madani et all[13]: This study compares traditional and integrated winglets. The results show the superiority of the integrated type, as it reduces drag and increases stability. The study relied on a detailed flow analysis and recommends using the integrated design.

DPR Babu et all[14]: This comprehensive study examines the impact of winglets on aerodynamic efficiency. The results demonstrate an overall improvement in performance, along with reduced fuel consumption and emissions. The study utilizes advanced CFD simulation technology and confirms that winglets are a fundamental component of modern aircraft design.

AL Gray and DW Zingg [15]: This study focuses on the design and optimization of blended winglets using a CFD methodology based on the RANS (Reynolds-Averaged Navier-Stokes) equations. The effect of winglet geometry, particularly can't angle and curvature, on wing aerodynamic performance was analysed. The results showed that using blended winglets significantly reduces induced drag while increasing the lift-to-drag ratio (L/D). Pressure distribution and flow lines around the wing were also analysed, demonstrating improved reduction in wingtip vorticity. The study confirms that combining CFD with engineering optimization techniques allows for a design that is both performance- and fuel-efficient.

I.3 A brief history of Air foil:

The word "aerofoil" is derived from a combination of the Greek words "aerios" meaning air and "foil" meaning blade. Since then, aerofoils have been developed and refined to the point where modern passenger aircraft can travel at speeds more than 500 mph. In this article, we will take a look at the historical development of aerofoil from its earliest days up to the present day. we have looked at the history of aircraft wings, and some of the key innovations that have taken place over the years. We have seen how different designs and materials have been used, and how aircraft wings have evolved to become the most important part of an aircraft. Aerofoil is a lifting surface, which extends along the leading edge and trailing edge of an aircraft wing. Modern aerofoils are very thin, typically about 0.1 inches, and generally are about ten percent thicker at their leading edge than at their trailing edges first successful attempt to create an aerofoil was made by Otto Lilienthal in 1891 [16].

Lilienthal who was born in Germany, in 1848 showed an early interest in aviation and began experimenting with glider designs in the late 1800s. His 1891 aerofoil design was the first to provide lift and stability in flight. Lilienthal's gliders were not controllable, and he frequently crashed during his flights. However, he continued to experiment and test new designs, publishing his findings in journals and at aviation meetings. In 1896, Lilienthal was fatally injured while flying a glider. Nevertheless, his work had a significant impact on the development of aviation. Lilienthal was a German aviation pioneer, and his design incorporated a cambered air foil shape which improved the lift-to-drag ratio of the aircraft.

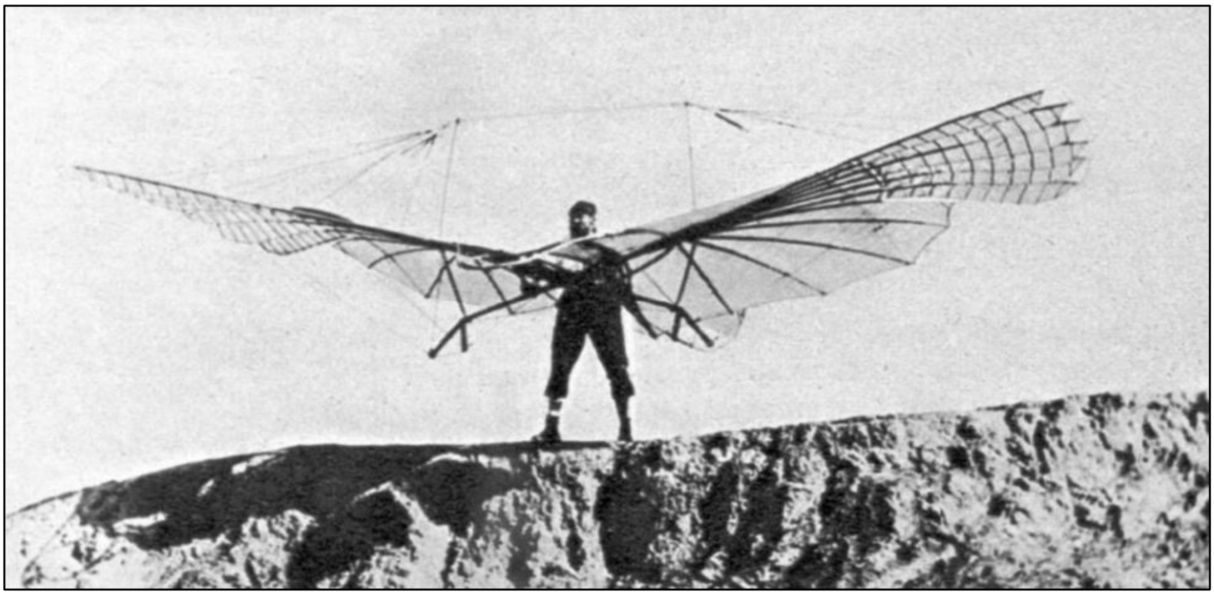

Fig 04: Lilienthal preparing for a Small Ornithopter flight, 16 August 1894 **[20]**

The first aerofoils were low sweepback wings designed to create a high degree of lift over the main wing. However, they were limited to low-speed flying. Aerofoils at this time were fairly basic in design and were not very efficient. They were made up of a single flat surface, and provided little lift or stability. This made them unsuitable for use in modern aircraft, which require greater levels of stability and performance [17].

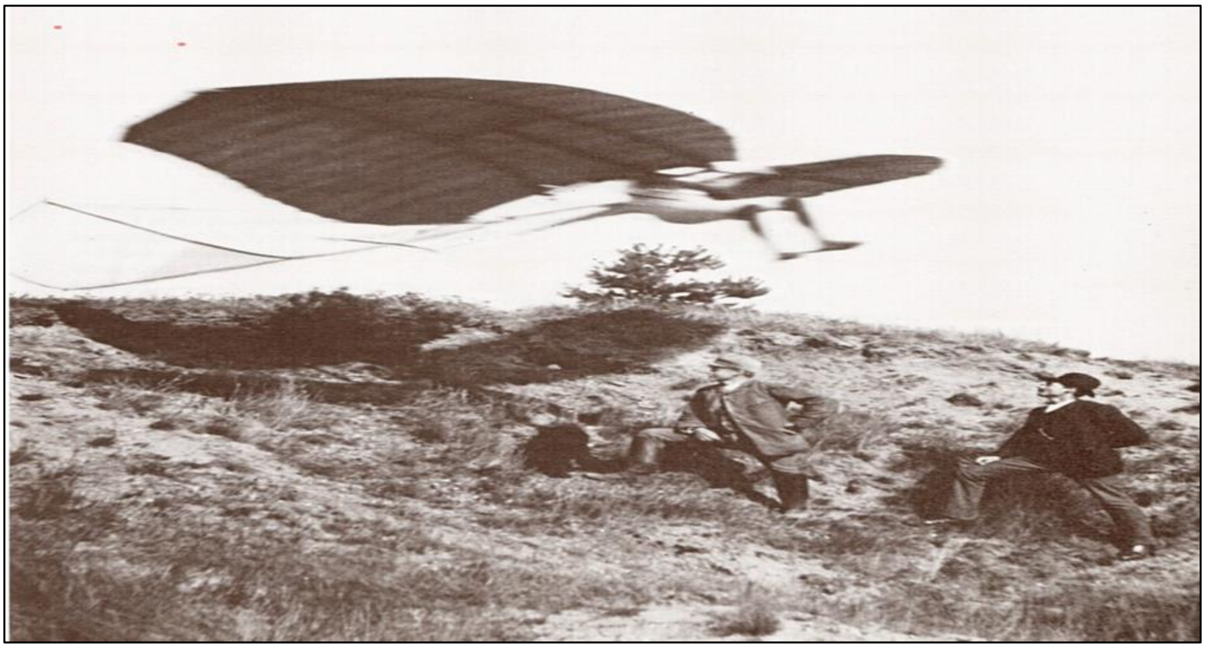

Fig 05: Flight attempt of Lilienthal on the DeRuiter Glider, Drewitz, 1891 [20]

The Wright brothers were the first to design and build an aircraft that used a lifting aerofoil, which they did in 1903. The Wright Brothers' Wright Flyer had a trapezoid-shaped wing with a thick, rigid spar that ran down the length of the wing. The wing was a single, flat surface, and was attached to the fuselage by a long, rigid strut. The Wright Flyer was designed with a strong, rigid backbone so that it could carry the weight of the pilot and passengers. The Wright Brothers' design was similar to Lilienthal's glider, but the Wright Flyer had a modest level of stability. The EDWARDIAN ERA is considered the era of progressive reforms in the US, in the same era, a government agency called NACA (National Advisory Committee for Aeronautics) was founded in 1915 to promote aeronautical research. It became the National Aeronautics and Space Administration (NASA) after World War II, NACA's first research laboratory was established in 1917 at Langley Memorial Aeronautical Laboratory, now part of Langley Research Centre. The agency's early work in fluid dynamics is still cited in modern textbooks [18].

Fig 06: The 1900 and 1902 Wright Gliders (reproductions) are hung in the new "Wright Brothers & The Invention of the Aerial Age" gallery, November 3, 2021. (Smithsonian photo by Jim Preston)[20]

Among other things, NACA developed the 4-digit and 5-digit series air foils which are still in use today. The NACA 4-digit series was developed in 1912 by NACA to provide a universal unit of length for aerofoils that would be used for defining the aerofoil shapes. This was done using the diameter of the aerofoil, which was easily measured in the manufacturing process. By using the measured diameter of the aerofoil, the NACA 4-digit series was able to define the aerofoil shape. The 4-digit series was introduced in the 1930s to replace the original NACA air foils for conventional air foils. The 4-digit series air foils are used on the majority of general aviation aircraft, as well as on most military aircraft. It is usually paired with the 5-digit series. The 4-digit series started with a 50-degree camber, which was later replaced with a slightly cambered air foil, and has been revised to include various air foils such as a camber-free air foil. The H-34A is a camber-free air foil and is one of the most widely used air foils in the world. The H-34A air foil has a wing area of around 15 square meters. The 4-digit series air foils have a leading slope of 5.5° and a trailing slope of 5.0°.

NACA 5-digit numbers were used from 1941 to 1978 when NASA adopted a five-digit system. In today's nomenclature, the five-digit numbers have been replaced by the NASA Standard Key Number, or more commonly the NASA Vehicle and Flight Data Number. The existing aerofoils are the most efficient variant which is the result of uninterrupted research and innovation which is still going on, the most recent and important study, which was funded by the European Union's Horizon 2020 research and innovation program, was conducted by a consortium of European universities and companies. It was led by the University of Bristol and involved the University of Sheffield, the University of Bristol, the University of Leicester, the University of Bari, and the National Institute of Aerospace Technology (INTA) in Madrid[19].

Definition of Airfoils:

An air foil is a two-dimensional cross-sectional shape of a three-dimensional wing, oriented parallel to the airflow. While a simple flat plate can generate lift when angled relative to the free airflow, air foils are typically designed with specific curvature and thickness to optimize lift generation efficiency and minimize aerodynamic losses.

The shape of the air foil is a fundamental element of wing design, significantly impacting the aircraft's aerodynamic characteristics and performance. Therefore, several basic air foil shapes are used depending on the specific performance requirements.

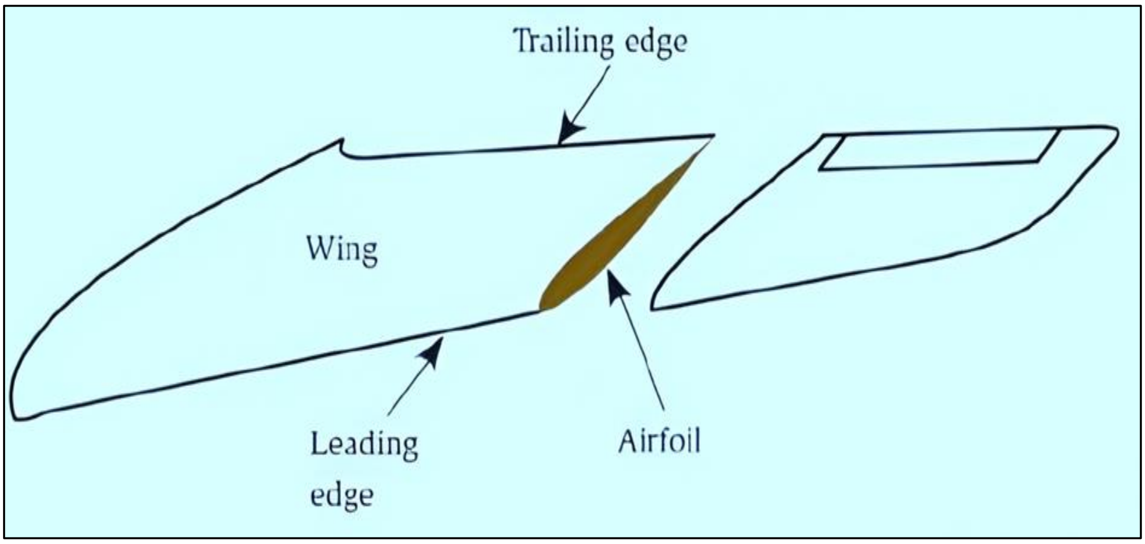

***Fig 07: Air foil Section*[21]**

I.4 Types of Airfoils:

Symmetric Airfoils: A symmetric air foil is characterized by the absence of camber, meaning that its curvature is identical on both the upper and lower surfaces with respect to the mean camber line. In this case, the chord line coincides with the camber line. As a result, a symmetric air foil does not generate lift when the angle of attack is zero.

Cambered Airfoils: In contrast to a symmetric air foil, a cambered air foil can generate lift even at zero or slightly negative angles of attack due to its curved shape. As the camber increases, the lift coefficient becomes higher; however, the critical angle of attack decreases compared to an air foil with less camber.

Supercritical air foils: A supercritical air foil is designed to minimize drag in the high subsonic flight regime, where portions of the airflow over the wing may locally reach supersonic speeds. Its geometry is characterized by a reduced curvature along the mid-chord region of the upper surface, creating a flatter profile compared to conventional air foils. Additionally, it features increased camber near the trailing edge, which enhances its load-carrying capability relative to traditional air foil designs.

Supersonic air foils: Supersonic air foils are designed according to different criteria compared to subsonic ones in order to achieve efficient performance at high-speed flight conditions. Nevertheless, their aerodynamic behaviour at low speeds is generally poorer than that of subsonic air foils.

Their geometry typically features a biconvex (symmetric) shape with sharp leading edges or very small radii of curvature. They are also characterized by a thin profile with a low thickness-to-chord ratio, and the maximum thickness is positioned further back along the chord. This design helps maintain a favourable pressure distribution over most of the wing surface, thereby reducing drag.

In addition, double-wedge air foil configurations are commonly used for aircraft operating at very high Mach numbers, particularly in supersonic research and high-speed applications.

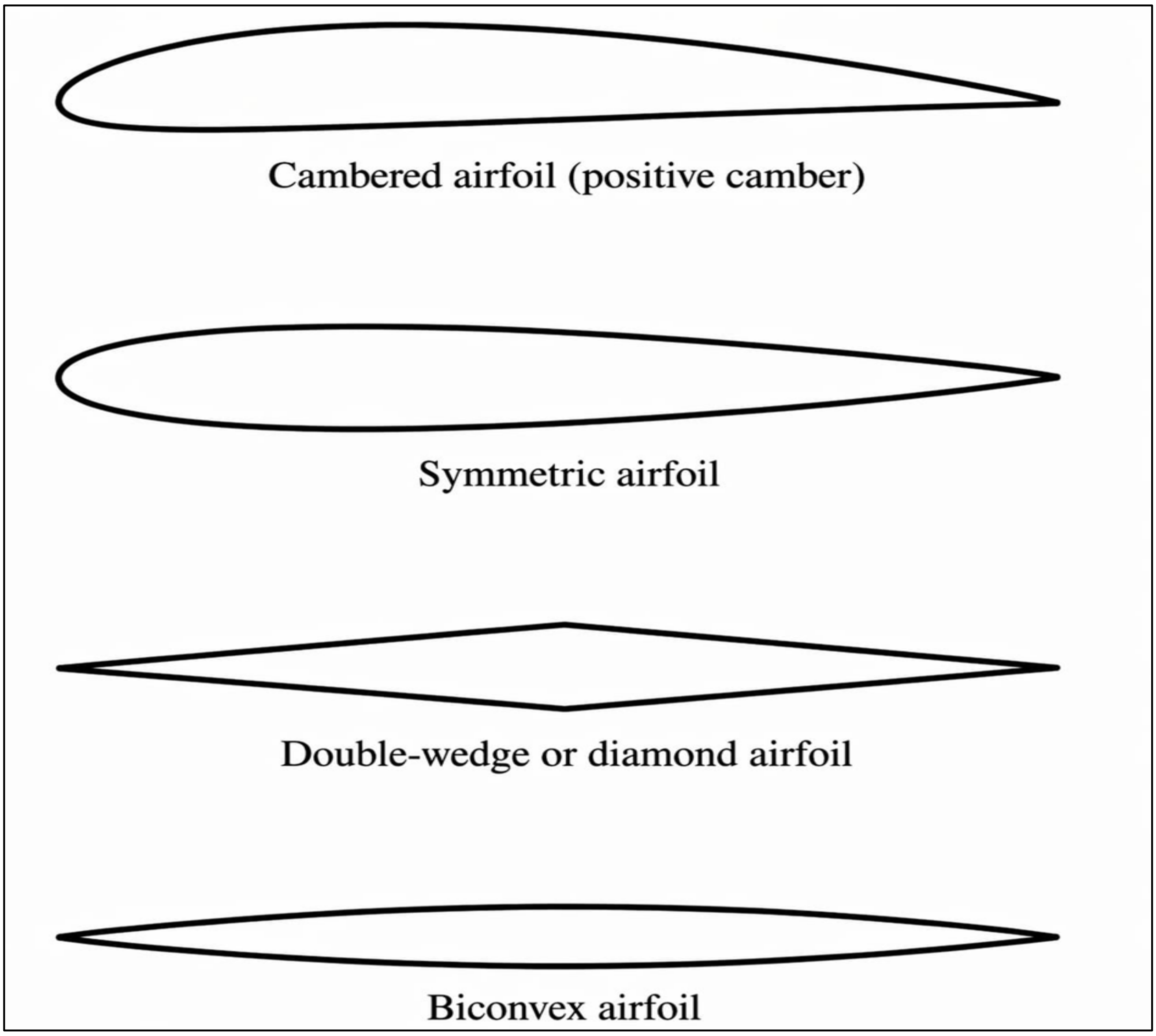

Fig 08: various air foil shapes[22]

Airfoils Profiles:

NACA: National Advisory Committee for Aeronautics is a major development in aerofoil design. The four- and five-digit series were created using analytical equations that determined the curvature of the centreline and the thickness distribution along the winglet. More recent series, such as the six-digit series, rely on more complex theoretical methods rather than straightforward geometric approaches. Prior to NACA's development of these series, winglet design depended heavily on experience and experimentation without clear mathematical rules. However, with the publication of a 1930 report analysing 78 different winglets, it was discovered that the most important factors were the curvature of the centreline and the thickness distribution. From this, equations were developed that allowed for the generation of entire families of aerofoil shapes, and these fundamental parameters have remained in place in all subsequent series. And ils types are NACA 4-Digit et NACA 5-Digit et NACA 6-Series et NACA 7-Series et NACA 8-Series[23]

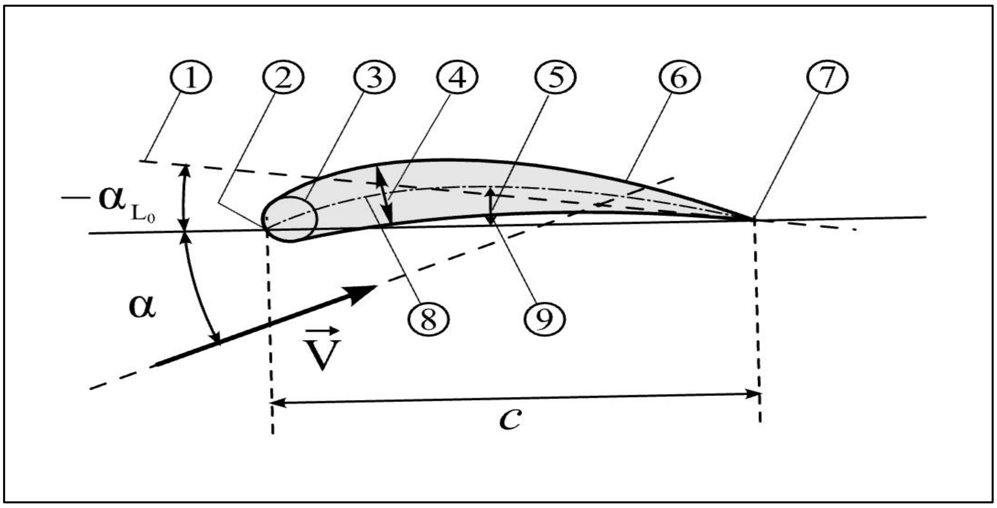

Fig 09: Types of NACA [23]

Clark Y Airfoils: The Clark Y air foil is a conventional wing section developed in the early 20th century within NACA research. It features a simple geometry combining a nearly flat underside and a convex topside, resulting in good lift generation with moderate drag. Its key characteristics include ease of fabrication, aerodynamic stability, and balanced performance at various angles of attack, achieving a suitable lift coefficient without complex design. In terms of applications, it has been widely used in light aircraft and prototypes, and is a fundamental section in wind tunnel testing and academic aerodynamic studies, particularly in performance optimization research such as drag reduction or increased aerodynamic efficiency [24].

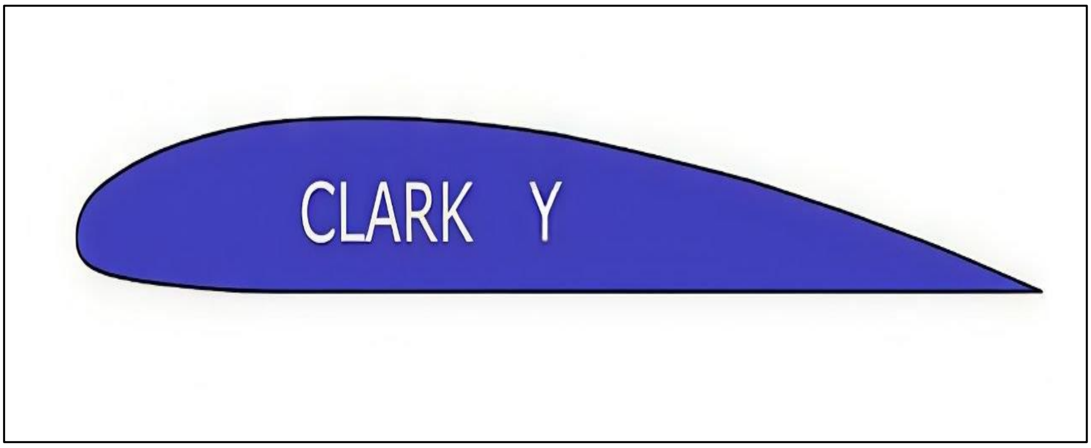

Fig 10: Clark Y air foil [24]

RAF (Royal Aircraft Factory Air foil):is the United Kingdom’s air and space force, established on 1 April 1918 through the amalgamation of the Royal Flying Corps and the Royal Naval Air Service, making it the world’s first independent air force. It is characterized by multi-domain capabilities that include air combat operations using advanced aircraft such as Typhoon and F-35 Lightning, intelligence, surveillance and reconnaissance (ISTAR), strategic airlift with platforms like C-17 and A400M Atlas, airborne early warning systems such as Wedgetail, as well as space and cyber operations. The RAF plays a critical role in defending UK and NATO airspace through Quick Reaction Alert (QRA), while also conducting humanitarian and relief missions and supporting international security operations across multiple continents. Its headquarters is located at RAF High Wycombe, and it operates through an organized structure of combat, support, training, and multi-domain operational groups [25].

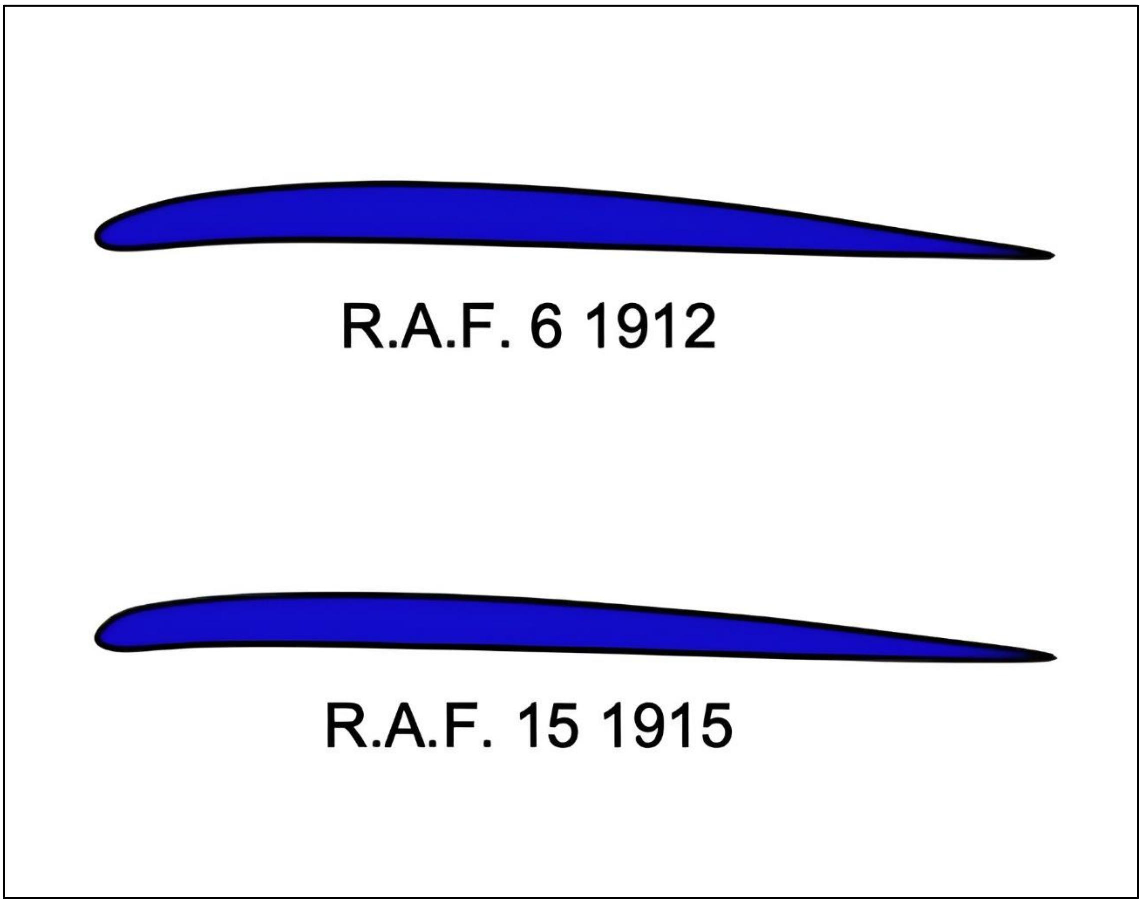

***Fig 11: Two streamlined sections of an aircraft wing RAF*[26]**

Selig S1223:

The Selig S1223 airfoil is classified in the scientific literature as a high-lift airfoil designed specifically for operation at low Reynolds number conditions. It is characterized by its ability to generate significantly higher lift compared to conventional Airfoils, making it suitable for light aircraft, unmanned aerial vehicles (UAVs), and low-speed flight applications. Experimental and computational studies have shown that it achieves high lift coefficients and performs well at high angles of attack, in addition to providing favorable characteristics for short takeoff performance and efficient flight under low-speed aerodynamic conditions[27].

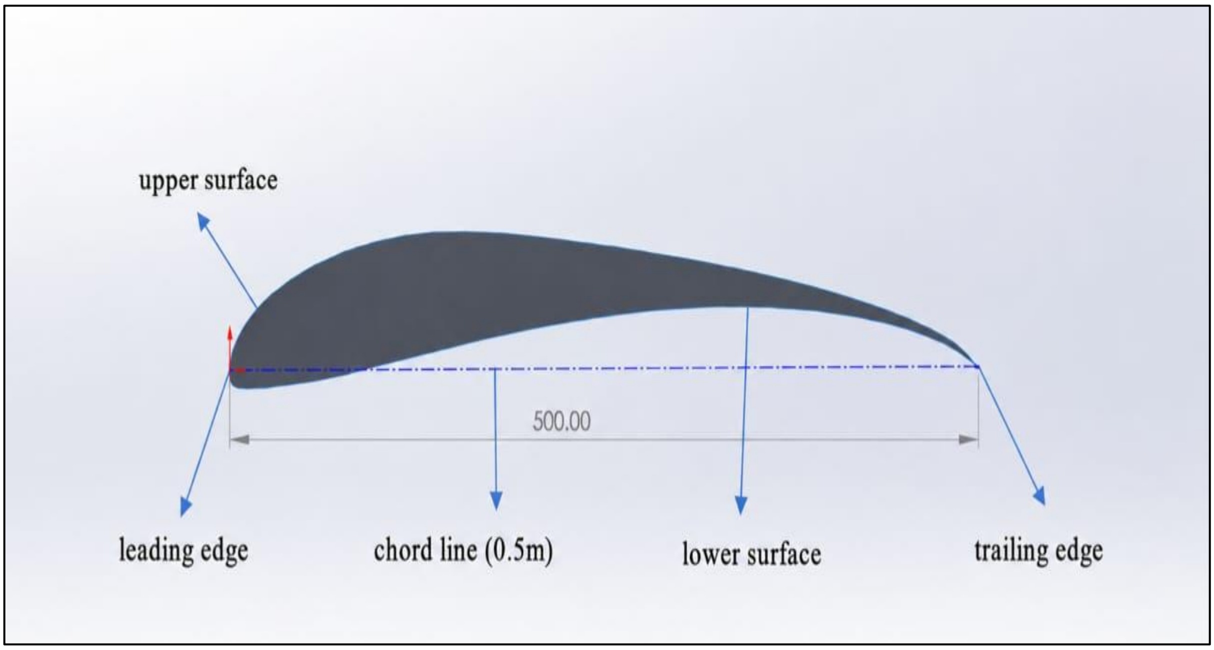

Figure 12: A standard Selig S1223 Airfoil[27]

Wing NASA:

NASA wing is a term used to refer to a group of airfoil shapes developed by the NASA through experimental aerodynamic research programs aimed at improving aircraft performance. These developments focus on enhancing aerodynamic efficiency by increasing lift and reducing drag, as well as improving airflow behavior around the wing across different flight regimes, including subsonic and supersonic speeds. These designs are based on advanced analytical and experimental methods used to study phenomena such as early flow separation and the effects of shock waves. This research has led to important innovations such as the supercritical wing, which significantly contributed to improving fuel efficiency and the stability of modern aircraft[28].

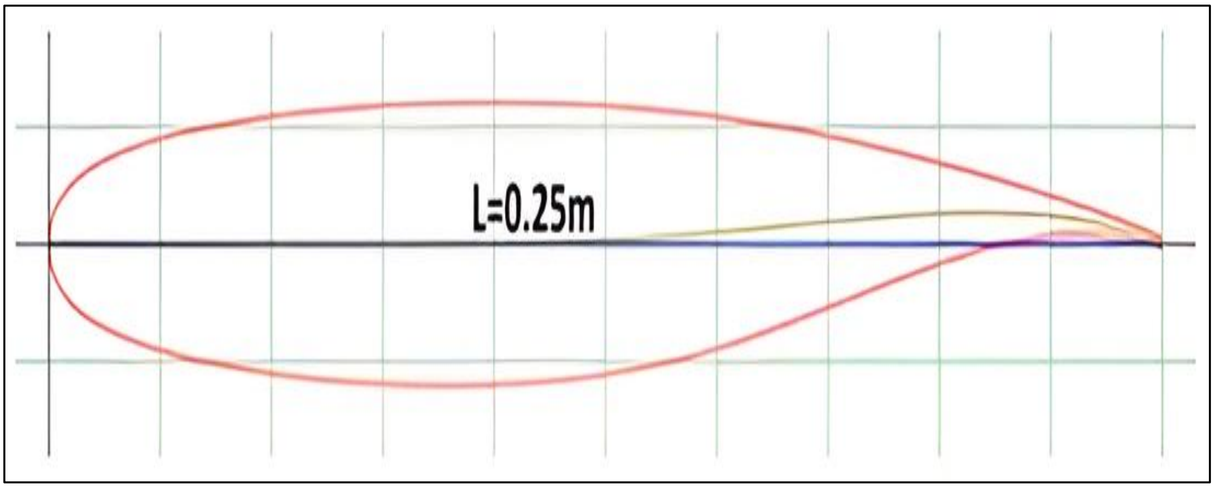

Fig 13: General view of NASA SC (2)-0714 airfoil [29]

Conclusion:

In conclusion, this research demonstrates that winglets are a fundamental element in aircraft design, directly impacting lift, stability, and overall flight efficiency. The study revealed that different winglet shapes lead to significant performance variations, making the design process a delicate balancing act between minimizing air resistance and maximizing lift.

Furthermore, the NACA winglet series is considered one of the most important reference models in aeronautical engineering due to its precision and widespread use in numerous aviation applications. Ultimately, understanding the characteristics of winglets is crucial for developing more efficient and advanced designs in the future, thus contributing to the advancement of the modern aviation industry.

Chapter II

Generalities on flow around an airfoil

II .1 Introduction

This chapter presents the theoretical and mathematical foundations of aerodynamics that are essential for understanding airflow behavior around airfoils. It introduces the fundamental aerodynamic forces acting on an airfoil, including lift, drag, and pitching moment, as well as the corresponding aerodynamic coefficients used to evaluate airfoil performance. Furthermore, the governing equations of fluid flow, namely the Navier–Stokes equations and their Reynolds-averaged form (RANS), are discussed. Particular attention is given to turbulence modeling through the SST k–ω model, which is widely used in computational fluid dynamics due to its accuracy in predicting complex turbulent flows. In addition, important dimensionless parameters such as the Reynolds number are presented, together with an overview of the major turbulence simulation approaches, including RANS, LES, and DNS. These theoretical concepts provide the necessary framework for the numerical simulations and aerodynamic analyses carried out in the following chapters.

II .2 Definition of Aerodynamics:

Aerodynamics is the science that studies the motion of air around bodies. In other words, it deals with the phenomena that occur whenever there is relative motion between a body and the surrounding air.

The body may move through a stationary fluid, such as an airplane in flight, or it may remain stationary while the fluid moves around it, such as a model in a wind tunnel [30].

II.3 Aerodynamic Force and Moment:

When air flows around an aircraft or any other body, it is forced to deviate from its original path, which causes variations in its velocity. According to Bernoulli’s principle, these velocity changes result in modifications of the pressure exerted by the airflow on the aircraft compared to the undisturbed stream. Moreover, the viscosity of air generates frictional effects that oppose the motion of the flow.As a consequence of these effects, the aircraft is subjected to a net aerodynamic force and moment. The most significant of these are lift, drag, and pitching moment. For analysis purposes, it is convenient to express these aerodynamic quantities in a non-dimensional form.

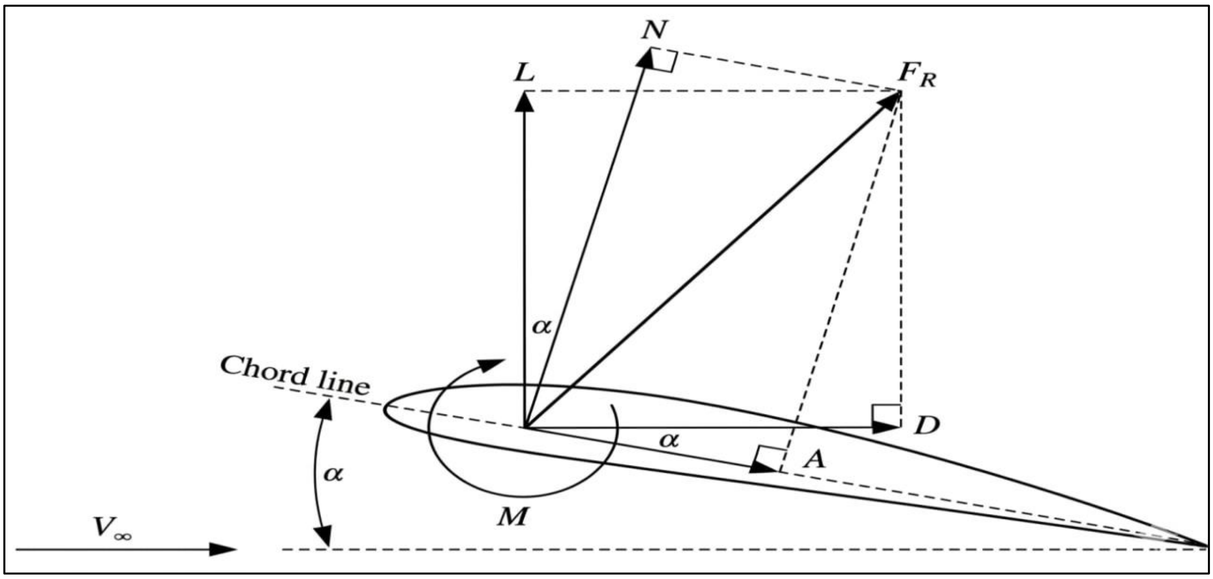

Fig 13: Aerodynamic forces on an airfoil.

The force coefficient C_F is defined by normalizing the aerodynamic force **F** using the freestream dynamic pressure q_∞ and a reference area S_{ref}, which is usually taken as the wing planform area of the aircraft[31].

$$C_F = \frac{F}{q_\infty S_{ref}} = \frac{F}{\frac{1}{2}\rho_\infty V_\infty^2 S_{ref}} = \frac{\textbf{aerodynamic force}}{\textbf{dynamic force}} \quad \textbf{II-1}$$

Similarly, the moment coefficient is defined as [31]:

$$C_M = \frac{F}{q_\infty C_{ref} S_{ref}} = \frac{F}{\frac{1}{2}\rho_\infty V_\infty^2 C_{ref} S_{ref}} = \frac{\textbf{aerodynamic momen}}{\textbf{dynamic moment}} \quad \textbf{II-2}$$

Where C_{ref} is the moment reference length, which is typically the wing chord length for an airplane. The non-dimensional aerodynamic coefficients area function of Reynolds number and Mach number, making them particularly useful in comparing different geometries and flows.

II.3.1 Lift:

Lift is the component of this force that is perpendicular to the oncoming flow direction. It contrasts with the drag force, which is the component of the force parallel to the flow direction. Lift conventionally acts in an upward direction in order to counter the force of gravity, but it can act in any direction at right angles to the flow [31].

$$L = \frac{1}{2} \rho \, S \, V^2 C_L \quad \textbf{II-3}$$

$$C_L = \frac{2L}{\rho \, S \, V^2} \quad \textbf{II-4}$$

II.3.2 Drag:

This is the component of force acting in the opposite direction to the line of flight, or in the same direction as the motion of the undisturbed stream. It is

the force that resists the motion of the aircraft. There is no ambiguity regarding its direction or sense [31].

$$D = \frac{1}{2} \rho \, S \, V^2 \, \boldsymbol{C_D} \quad \textbf{II-5}$$

$$C_{\boldsymbol{D}} = \frac{2D}{\rho \, S \, V^2} \quad \textbf{II-6}$$

II.4 Pressure coefficient:

The pressure acting over the surface area of a body makes an important contribution to the aerodynamic force on the body. The pressure is a dimensional quantity with units of force per unit area, such as N/m2 in SI units and lb/ft2 in English units. We define a dimensionless pressure coefficient as[31]:

$$C_P = \frac{P - P_\infty}{q_\infty} \quad \textbf{II-7}$$

Where **p** is the local pressure, P_∞ is the freestream static pressure, and q_∞ is the freestream dynamic pressure.

II.5 Mathematical model:

II.5.1 Equations solved in steady state:

In this case, the profile is at a fixed angle of incidence. The study is done for an incompressible Newtonian flow (air) for turbulent flow at steady state.We will

consider a fluid dynamic in a wysterne with Catesian coordinates O(x,y)`, where $\vec{U}$(x,y)=(u,v) is the velocity vector. The equations of Narier-Stoks are done in 2D:

$$\frac{\partial u}{\partial x}+\frac{\partial v}{\partial y}=0 \quad \textbf{II-8}$$

$$u\frac{\partial u}{\partial x}+v\frac{\partial u}{\partial y}=-\frac{1}{\rho}\frac{\partial p}{\partial x}+\nu\left(\frac{\partial^2 u}{\partial x^2}+\frac{\partial^2 u}{\partial y^2}\right) \quad \textbf{II-9}$$

$$u\frac{\partial v}{\partial x}+v\frac{\partial v}{\partial y}=-\frac{1}{\rho}\frac{\partial p}{\partial y}+\nu\left(\frac{\partial^2 v}{\partial x^2}+\frac{\partial^2 v}{\partial y^2}\right) \quad \textbf{II-10}$$

Mean Navier-Stokes equations:

To simulate turbulent water, we use the Reynolds decomposition, the Reynolds mean used for incompressible flows[32][33] , which is the first approximation of the approximate value of turbulent flows[34]. The balance values are averaged either over time for pervasive problems or over a large number of figures, and only the average values are explicit. But since in many cases we are only interested in averages, this treatment is sufficient for most industrial problems[35] . Ea iatroduinnt la average Reynolds, les equations de Navler-Stokes pour in ecolemes s at loaaire woat 'erire comme sui:

$$\bar{u}\frac{\partial \bar{u}}{\partial x}+\bar{v}\frac{\partial \bar{u}}{\partial y}=-\frac{1}{\rho}\frac{\partial \bar{p}}{\partial x}+\nu\left(\frac{\partial^2 \bar{u}}{\partial x^2}+\frac{\partial^2 \bar{u}}{\partial y^2}\right)+\left(-\frac{\partial \overline{u'^2}}{\partial x}-\frac{\partial \overline{u'v'}}{\partial y}\right) \quad \textbf{II-11}$$

$$\bar{u}\frac{\partial \bar{v}}{\partial x}+\bar{v}\frac{\partial \bar{v}}{\partial y}=-\frac{1}{\rho}\frac{\partial \bar{p}}{\partial x}+\nu\left(\frac{\partial^2 \bar{v}}{\partial x^2}+\frac{\partial^2 \bar{v}}{\partial y^2}\right)+\left(-\frac{\partial \overline{v'^2}}{\partial y}-\frac{\partial \overline{u'v'}}{\partial x}\right) \quad \textbf{II-12}$$

The nonlinearity of the equations leads, in this approach, to the appearance of additional unknowns, which makes the classical system of equations underdetermined (the number of unknowns exceeds the number of equations). It is therefore necessary to formulate additional equations, known as closure equations, in order to solve the problem. This formulation corresponds to a modeling phase, namely turbulence modeling [36].

Turbulence equations: Turbulence models are applied to complete the system of equations to be solved. For our simulations, we use the SST k-ω turbulence model developed by Florian R. Menter [37]. This choice is motivated by its efficiency and accuracy in simulating flows with strong pressure gradients and complex applications compared to other models [38][39][40].

The SST k-ω turbulence model combines the k-ω turbulence model of David C. Wilcox with the k-ε turbulence model (formulated for high Reynolds numbers). This model aims to take advantage of both approaches: the k-ω model is used in the near-wall region (boundary layer sublayers), while the k-ε model is applied in regions far from the airfoil [34].

The SST k-ω turbulence model developed by Florian R. Menter is a two-equation model. To formulate it, the following parameters are defined [37]:

The turbulent kinetic energy k:

$$k=\frac{1}{2}\overline{u'_i u'_i} \qquad \text{II-13}$$

i= A dimension index equal to 1 for x and 2 for y.

The turbulence dissipation rate ϵ :

$$\epsilon = \nu \overline{\frac{\partial u'_i}{\partial x_j}} \overline{\frac{\partial u'_i}{\partial x_j}} \qquad \text{II-14}$$

The specific dissipation rate of turbulent kinetic energy ω:

$$\omega = \frac{\epsilon}{k} \qquad \text{II-15}$$

The equations' for k and ω are written as:

$$\rho u_j \frac{\partial k}{\partial x_j} = P - \beta^* \rho \omega k + \frac{\partial}{\partial x_j}\left[(\mu + \sigma_k \mu_t)\frac{\partial k}{\partial x_j}\right] \qquad \text{II-16}$$

$$\rho u_j \frac{\partial \omega}{\partial x_j} = \frac{\gamma}{\nu_t} P - \beta \rho \omega^2 + \frac{\partial}{\partial x_j}\left[(\mu + \sigma_\omega \mu_t)\frac{\partial \omega}{\partial x_j}\right] + 2(1 - F_1)\frac{\rho \sigma_{\omega 2}}{\omega}\frac{\partial k}{\partial x_j}\frac{\partial \omega}{\partial x_j} \qquad \text{II-17}$$

With:

$$P = \tau_{ij}\frac{\partial u_i}{\partial x_j} \qquad \text{II-18}$$

End

$$\tau_{ij} = \mu_t \left(\frac{\partial u_i}{\partial x_j} + \frac{\partial u_j}{\partial x_i}\right) - \frac{2}{3}\rho k \delta_{ij} \qquad \textbf{II-19}$$

Turbulent viscosity is defined by the following relationship:

$$\mu_t = \frac{\rho a_1 k}{\max(a_1 \omega, \Omega F_2)} \qquad \textbf{II-20}$$

The additional functions are defined by the following relationships:

$$F_1 = \tanh(arg_1^4) \qquad \textbf{II-21}$$

And

$$F_2 tanh(arg_2^2) \qquad \textbf{II-22}$$

With:

$$arg_1 = min\left[max\left(\frac{\sqrt{k}}{\beta^* \omega y}, \frac{500v}{y^2 \omega}\right), \frac{4\rho\sigma_{\omega 2} k}{CD_{k\omega} y^2}\right] \qquad \textbf{II-23}$$

$$CD_{k\omega} = max\left(2\rho\sigma_{\omega 2}\frac{1}{\omega}\frac{\partial k}{\partial x_j}\frac{\partial \omega}{\partial x_j}, 10^{-20}\right)$$

$$arg_2 = max\left(2\frac{\sqrt{k}}{\beta^* \omega y}, \frac{500v}{y^2 \omega}\right)$$

The values of the constants are:

$\beta^* = 0{,}09$ $\mathrm{k} = 0{,}41$ $a_1 = 0{,}31$

For the other constants, we apply the following general relationship:

$$\psi = F_1 \psi_1 + [1 - F_1]\psi_2 \qquad \textbf{II-24}$$

With:

$\gamma_1 = \frac{\beta_1}{\beta^*} - \frac{\sigma_{\omega 1} k^2}{\sqrt{\beta^*}}$ $\gamma_2 = \frac{\beta_2}{\beta^*} - \frac{\sigma_{\omega 2} k^2}{\sqrt{\beta^*}}$

$\sigma_{k1} = 0.850$ $\sigma_{\omega 1} = 0{,}5$

$\sigma_{k2} = 1{,}0$ $\sigma_{\omega 2} = 0{,}856$

$\beta_1 = 0{,}075$ $\beta_2 = 0{,}0828$

Number of Reynolds:

The Reynolds number (Re) is a dimensionless quantity used to describe the flow regime of a fluid moving around a solid body, such as an airfoil. It is defined as follows:

Reynolds Number = Inertial Force / Viscous Force

This dimensionless number expresses the balance between inertial forces and viscous forces acting on a fluid near a solid body. It is particularly important in the subsonic flow regime, where these two effects are dominant.

At low Reynolds numbers (low flow velocities), viscous forces dominate, and the flow is typically laminar and smooth. At high Reynolds numbers (high velocities), inertial forces become more significant, leading to unstable and chaotic motion known as turbulent flow.

In general, the Reynolds number provides a physical characterization of the flow by indicating its regime (laminar, transitional, or turbulent). It quantifies the relative influence of inertia compared to viscosity in fluid motion, making it one of the key dimensionless parameters in fluid dynamics [41].

$$R_e \frac{\rho V L}{\mu} \quad \textbf{II-24}$$

The Reynolds number equation is used to relate the fluid's velocity, characteristic length (such as diameter), and viscosity. The type of flow is determined according to the value of Re.

- If Re < 2000, the flow is called Laminar
- If Re > 4000, the flow is called turbulent
- If 2000 < Re < 4000, the flow is called transition.

The major classes of turbulence modelling:

There is no single, comprehensive theoretical framework that fully explains turbulence. Instead, the study of this field relies on a range of approximate models and partial theories. Some of these models are relatively simple and limited in their application, yet remain useful in engineering and industrial applications, while others are more complex and require advanced mathematical formulations. Generally, turbulent flow can be represented using three main approaches: direct numerical simulation (DNS), which solves all scales of motion without any modeling; large-scale vortex simulation (LES), which solves only large-scale turbulent structures while modeling small scales; and average-value-based methods such as Reynolds models (RANS), which describe the average behavior of flow without tracking instantaneous

scillations [41].

Simulation of Navier stokes Averaging Equations (RANS):

The Navier-Stokes equations-based Reynolds Average (RANS) method relies on solving the time-averaged form of the Navier-Stokes equations, meaning that turbulence effects are not directly solved but rather fully modeled. Consequently, the accuracy of the results may be limited and may not always reflect the true behavior of turbulent flow, especially in highly complex cases. However, this method provides reliable estimates of average flow values such

as velocity, temperature, and pressure. For this reason, many industrial computational fluid dynamics (CFD) programs are based on the RAN framework. Furthermore, its relatively low computational cost in terms of processing time makes it suitable for simulating complex geometries usingm precisecomputational networks [42].

Direct Numerical Simulation (DNS):

The Reynolds-Averaged Navier–Stokes (RANS) approach is based on solving the time-averaged form of the Navier–Stokes equations, in which the effects of turbulence are not explicitly resolved but instead modeled through turbulence closures. Consequently, prediction accuracy can be limited, particularly in flows with strong unsteadiness or complex turbulent structures. Despite these limitations, RANS models remain highly effective for predicting mean flow quantities such as velocity, temperature, and pressure. Owing to their balance between accuracy and computational efficiency, RANS methods are widely used in industrial computational fluid dynamics (CFD) applications. Their relatively low computational cost also makes them well suited for simulations involving complex geometries and fine numerical meshes [42].

Large Eddy Simulation (LES):

Large Eddy Simulation (LES) solves a spatially filtered form of the Navier–Stokes equations, where the large turbulent structures are directly resolved while the smaller scales are modeled. In practice, this filtering is implicitly controlled by the computational mesh: flow structures larger than the grid resolution are computed explicitly, whereas the smaller, subgrid-scale motions are represented using turbulence models. To account for these unresolved small-scale effects, so-called subgrid-scale (SGS) models are introduced to approximate their influence on the resolved flow. One of the main advantages of LES is that it provides access not only to mean flow quantities but also to time-dependent fluctuations, which makes it more informative than RANS methods for unsteady turbulent phenomena.

Although LES is significantly more computationally demanding than RANS, its cost remains far lower than DNS, making it a practical compromise for simulating complex geometries with reasonably refined meshes [42].

Conclusion

In this chapter, the fundamental principles of aerodynamics and fluid mechanics relevant to airfoil analysis have been reviewed. The concepts of lift, drag, pressure coefficient, and aerodynamic moments were presented to characterize the aerodynamic behavior of airfoils. The mathematical formulation based on the Navier–Stokes equations and Reynolds-averaged equations was also introduced, highlighting the importance of turbulence modeling in CFD simulations. The SST k–ω turbulence model was selected due to its capability to accurately predict flow separation and adverse pressure-gradient effects. Furthermore, the Reynolds number and the main numerical approaches for turbulence simulation were discussed. These theoretical foundations constitute the basis for the numerical methodology adopted in this study and provide the tools required to analyze and interpret the aerodynamic performance of the investigated airfoil configurations.

Chapter III

Simulation and results

III.1 Introduction

III.1.1 Geometry and Mesh

The first step in conducting a CFD simulation is to investigate the effect of mesh size on the solution results. While increasing the number of computational nodes generally improves numerical accuracy, it also raises memory requirements and computational time. The optimal number of nodes can be determined by progressively increasing them until the mesh is sufficiently refined such that further refinement no longer produces significant changes in the results.

This study found that a C-type grid consisting of 40,400 quadrilateral cells is sufficient to achieve a grid-independent solution, with the domain height set to approximately 15 chord lengths.

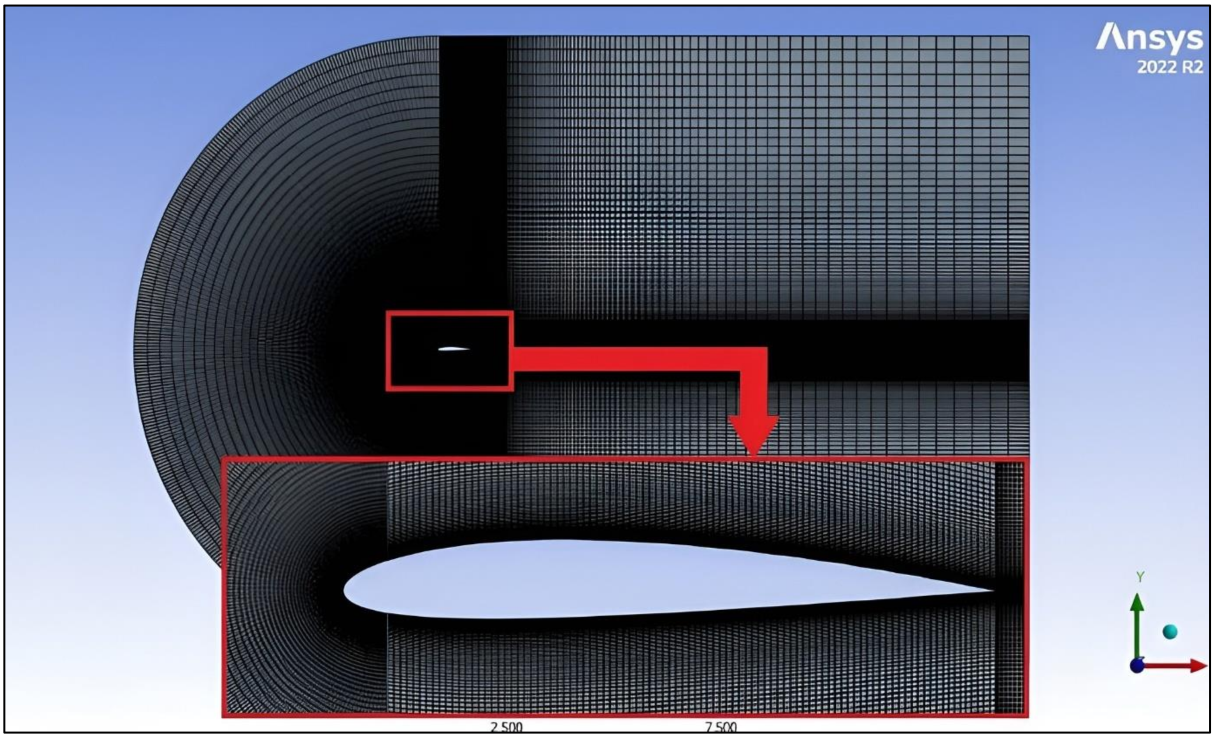

Fig 14: Mesh around NACA2412 airfoil

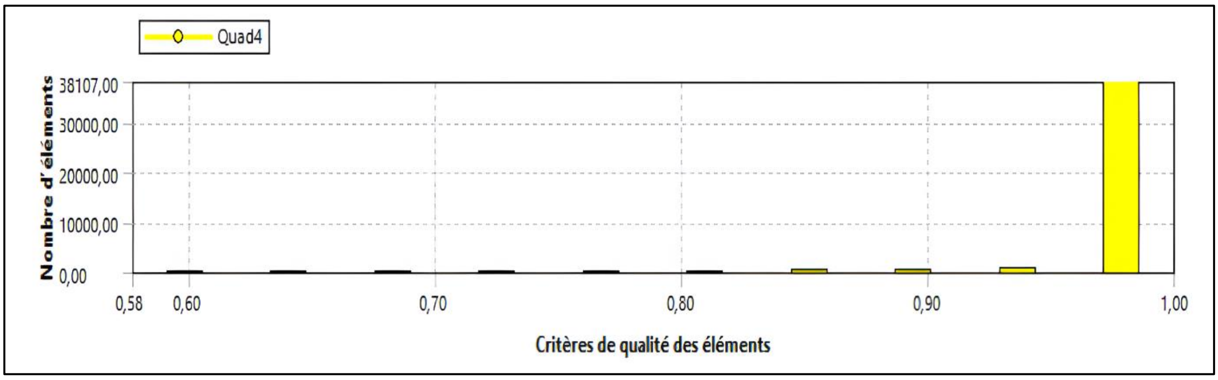

Fig 15: Mesh Orthogonal quality.

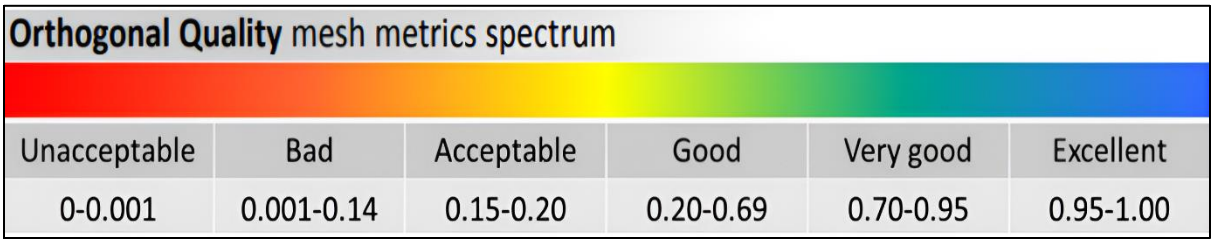

Orthogonal Quality mesh metrics spectrum

Unacceptable	Bad	Acceptable	Good	Very good	Excellent
0-0.001	0.001-0.14	0.15-0.20	0.20-0.69	0.70-0.95	0.95-1.00

Fig 16: Orthogonal Quality Mesh

Low orthogonal values or high inclination angles are generally undesirable in mesh generation. Typically, the minimum orthogonal quality is maintained above 0.1, while the maximum inclination should remain below 0.95. Nevertheless, these limits may vary depending on the physical model and the specific location of the mesh cell. A high-quality mesh is characterized by:

- The mesh quality criteria are in the correct range - Orthogonal quality.
- The mesh size is valid for the studied physics - Boundary layer.
- Important geometric details are well captured.

III.2 Results and Discussion

The aerodynamic behavior of the airfoil was analyzed at angles of attack of 0°, 5°, 10°, and 15°. The obtained results show that both the lift and drag coefficients vary significantly with the increase in angle of attack due to changes in the airflow behavior around the airfoil surface. At low angles of attack, the airflow remains relatively attached to the airfoil surface, resulting in low drag and moderate lift generation. As the angle of attack increases to 5° and 10°, the pressure difference between the upper and lower surfaces becomes larger, leading to a progressive increase in the lift coefficient while the drag coefficient also increases gradually. At 15°, the airfoil approaches the critical angle of attack where flow separation begins to occur on the upper surface, causing a rapid increase in aerodynamic drag and a reduction in airflow stability. Although the lift coefficient may reach values close to its maximum at this condition, further increase in angle of attack can lead to stall and a decrease in lift performance. The corresponding lift and drag coefficient curves presented in Figures 17 and 18 clearly illustrate the aerodynamic performance variation of the airfoil with angle of attack.

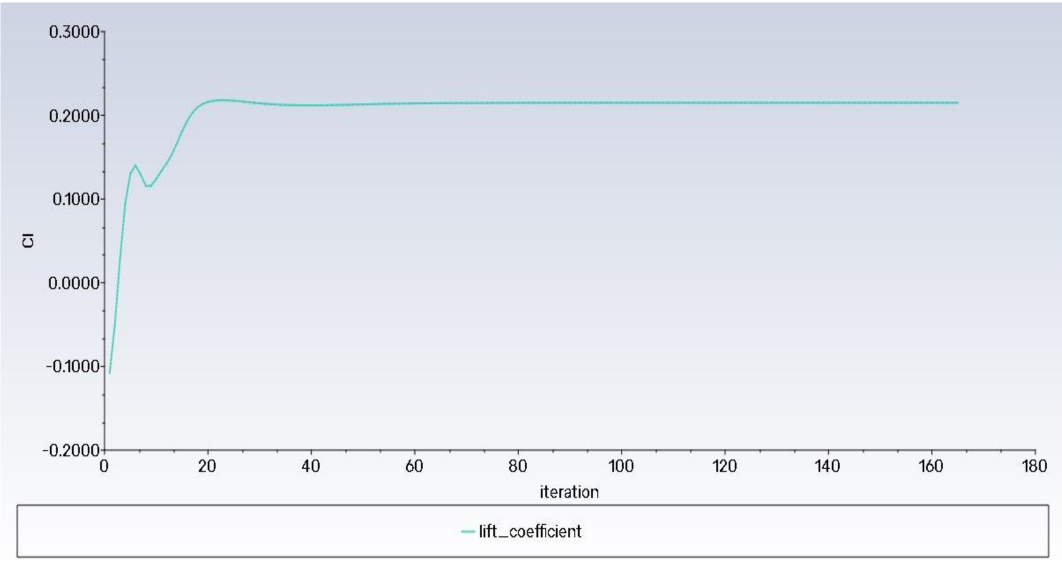

Fig 17: Coefficient of Lift versus AOA.

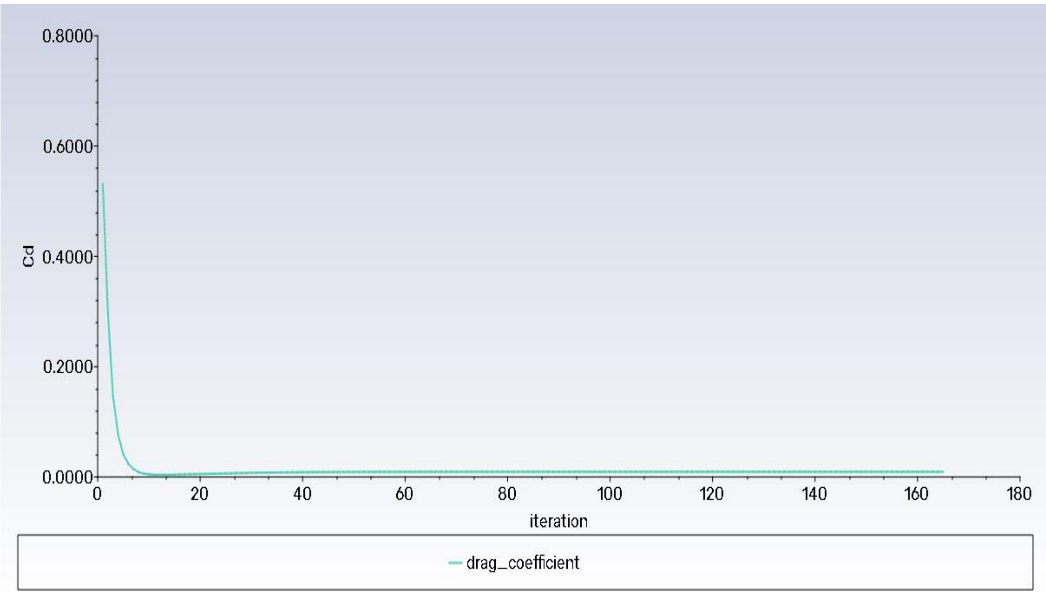

Fig 18: Coefficient of Drag versus AOA

Velocity contour

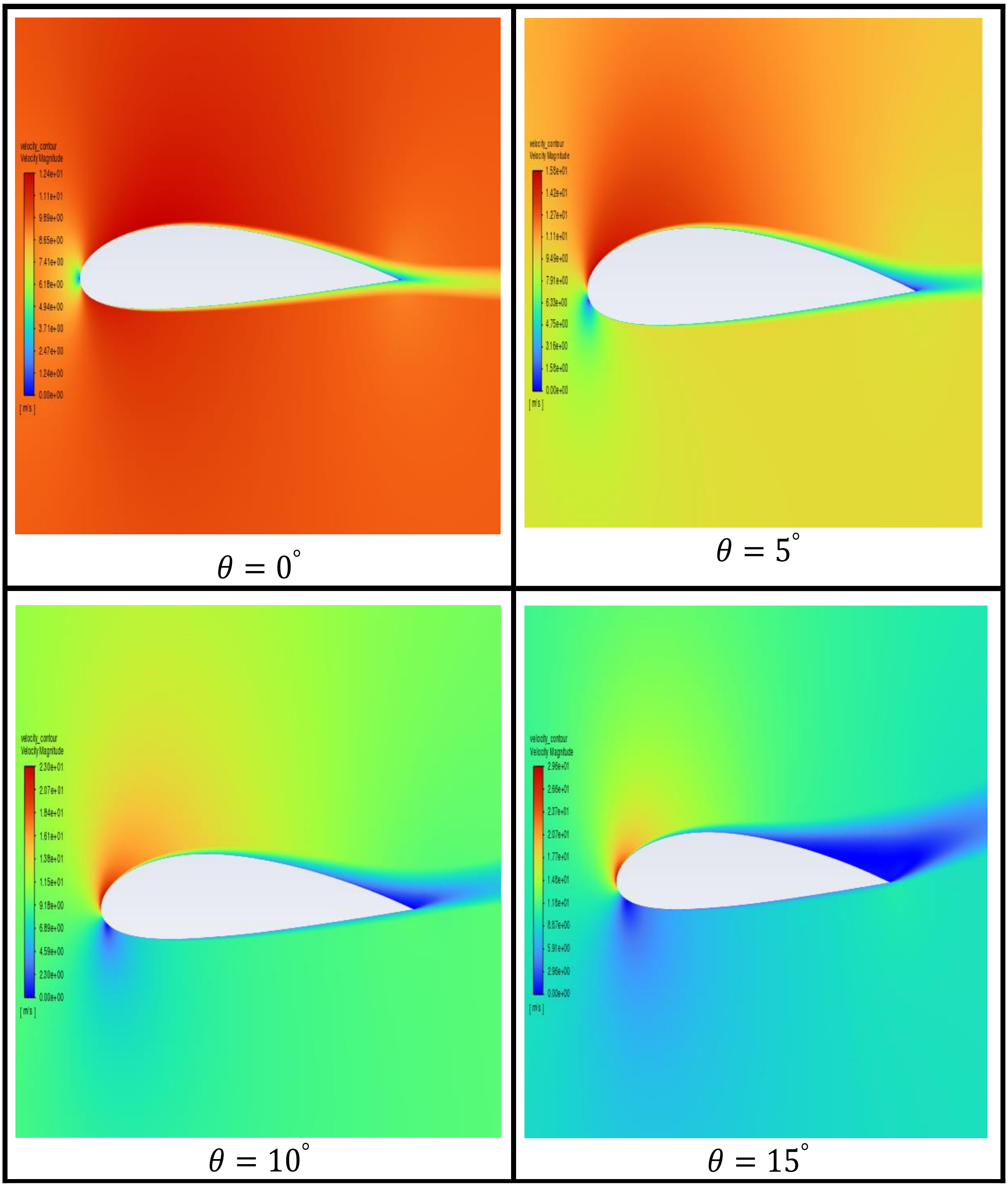

Fig 19: Velocity magnitude contours at an inlet velocity of 10 m/s

Comparison:

The images depict the velocity distribution around the wingtip at a constant velocity of $10 m/_{s}$ and at different angles of attack 0°, 5°, 10°, and 15°. As the angle of attack increases, the airflow behavior changes significantly, particularly in terms of velocity distribution, pressure differential, and lift. At an angle of attack 0°, the flow is relatively uniform around the wingtip, and there is a small difference in velocity between the upper and lower surfaces, resulting in low lift. Furthermore, the separation zone behind the trailing edge is very limited, indicating stable flow and low drag.

At 5°, the velocity on the upper surface begins to increase significantly due to the pressure drop, and a more pronounced difference appears between the two sides of the wing. This leads to increased lift while the airflow remains attached to the wing surface without significant separation, resulting in good and stable aerodynamic performance.

At 10°, the high-velocity areas become more pronounced above the upper surface, and the pressure differential increases considerably, significantly raising the lift value. However, signs of airflow separation begin to appear near the trailing edge, and a greater wake effect is observed behind the wing, indicating increased drag.

At 15°, the airflow becomes more turbulent, with the separation area expanding significantly above the upper surface and behind the wing. Although lift may be high, drag increases considerably, and the wing approaches a stall state, where the airflow becomes unstable and aerodynamic efficiency decreases.

- Higher flow velocity over the upper surface
- Increased pressure difference and therefore increased lift
- Expansion of the wake region behind the airfoil
- A gradual increase in drag
- Clear flow separation at high angles of attack15°

Therefore, the best aerodynamic performance is typically achieved at moderate angles of attack$5^{\circ}$and 10°, where a good balance exists between lift generation and flow stability, without entering stall conditions.

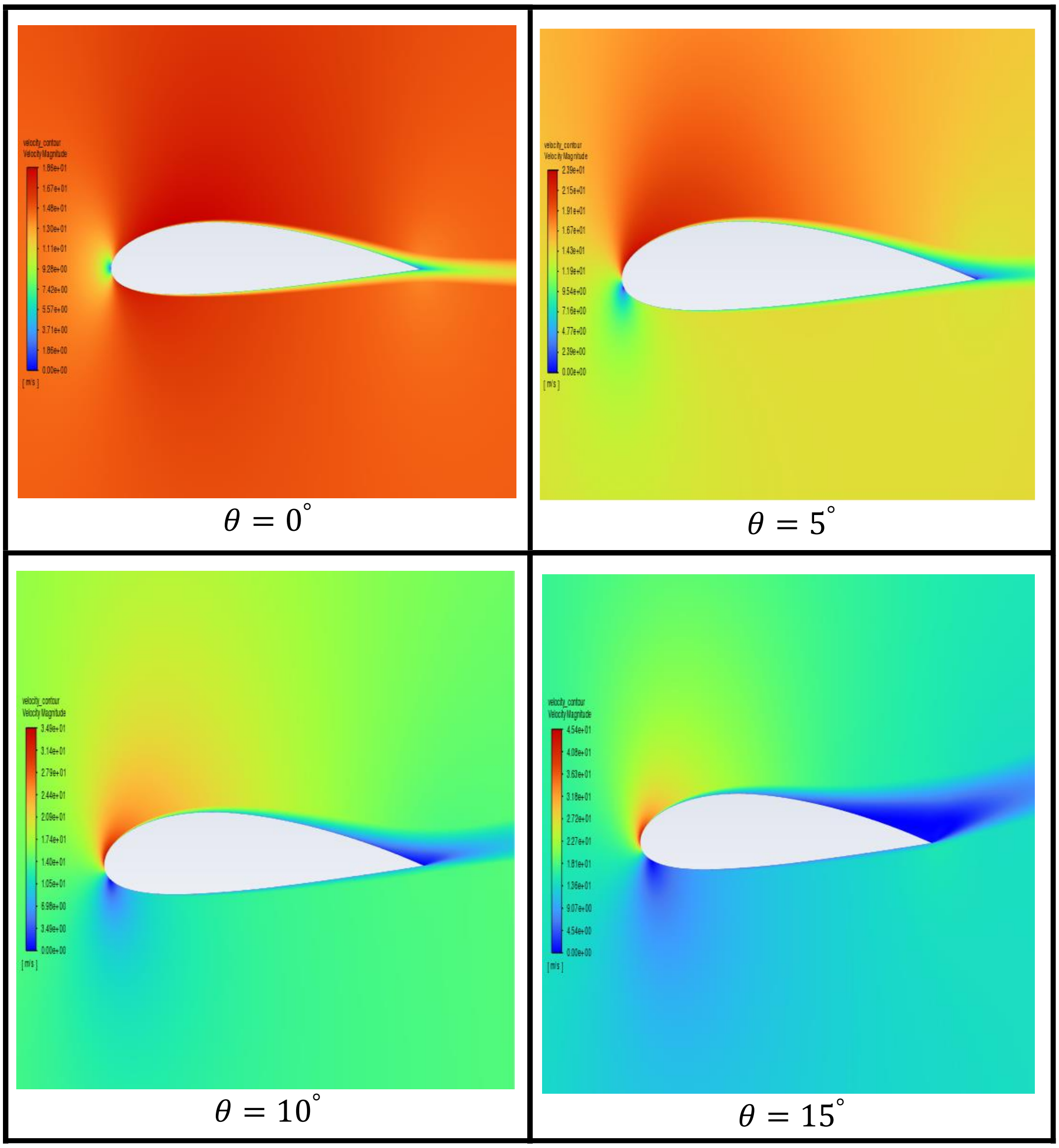

Fig 20: Velocity magnitude contour 15m/s

Comparison:

At a velocity of 15 m/s, the airflow behavior around the airfoil changes as the angle of attack increases. At 0°, the flow is smooth and stable with almost no flow separation and relatively low lift force. When the angle of attack increases to 5°, the airflow velocity over the upper surface increases, resulting in higher lift while maintining good aerodynamic efficiency and stable flow behavior. At 10°, the lift force increases further, and flow disturbances begin to appear behind the airfoil with partial flow separation near the trailing edge. At 15°, the flow separation becomes more significant, and the wake region behind the airfoil expands considerably, leading to a large increase in drag and a reduction in aerodynamic efficiency, indicating that the airfoil is approaching stall conditions.

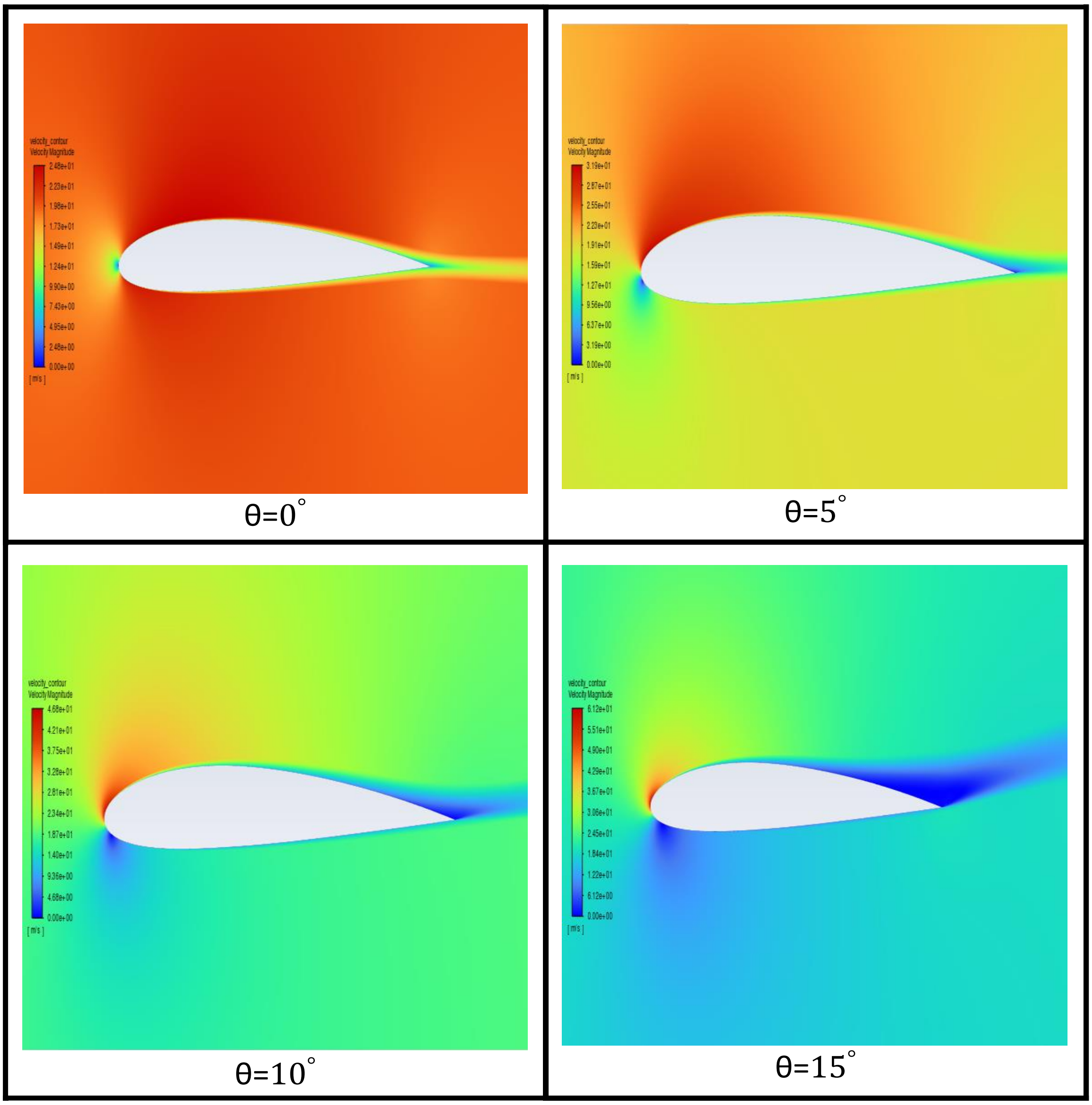

Fig 21: Velocity magnitude contour* 20 *m/s

Comparison:

At a velocity of $20\,{}^{m}/_{s}$, the contour results show a clear difference in the velocity distribution around the airfoil as the angle of attack increases. At an angle of attack of 0°, the airflow is almost symmetrical and stable around the airfoil, with only a very small wake region behind the trailing edge, indicating smooth flow and minimal disturbance. When the angle of attack increases to 5°, the airflow velocity over the upper surface increases due to the higher pressure difference, and a slight disturbance appears behind the airfoil, resulting in improved lift generation. At 10°, the velocity difference between the upper and lower surfaces becomes larger, and the wake region behind the airfoil extends further, indicating increased lift along with the beginning of more noticeable flow separation effects. At an angle of attack of 15°, a large separation region forms behind the airfoil with significant flow disturbance and less uniform velocity contours. This indicates that the airfoil is approaching stall conditions, where aerodynamic efficiency starts to decrease despite the higher angle of attack.

Pressure contours:

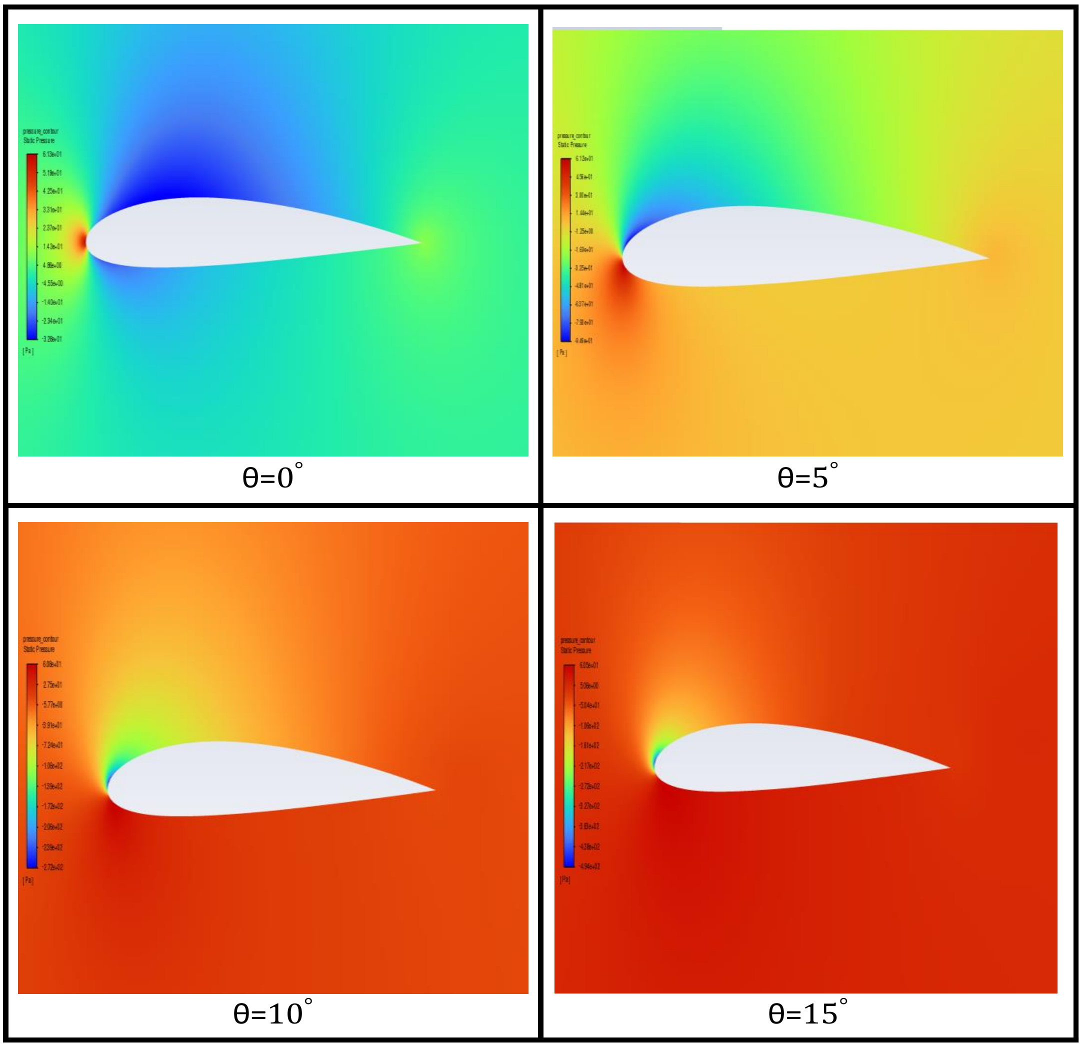

Fig 22: pressure contours 10 m/s

The images illustrate the pressure distribution around the airfoil at a constant velocity of 10 m/s and angles of attack of 0°, 5°, 10°, and 15°. At an angle of attack of 0°, the pressure distribution is nearly symmetrical between the upper and lower surfaces of the airfoil, resulting in a small pressure difference and limited lift force. When the angle of attack increases to 5°, the pressure on the upper surface decreases while the pressure on the lower surface increases, leading to a higher lift force. At 10°, the pressure difference becomes more significant, with a larger low-pressure region forming above the airfoil and higher pressure below it, which greatly enhances lift generation. At 15°, the largest pressure difference is observed, with a strong pressure drop on the upper surface and high pressure beneath the airfoil. However, signs of flow disturbance begin to appear near the leading edge, indicating that the airfoil is approaching flow separation or stall conditions. In general, increasing the angle of attack increases the pressure difference and lift force until a critical angle is reached, beyond which aerodynamic instability may occur.

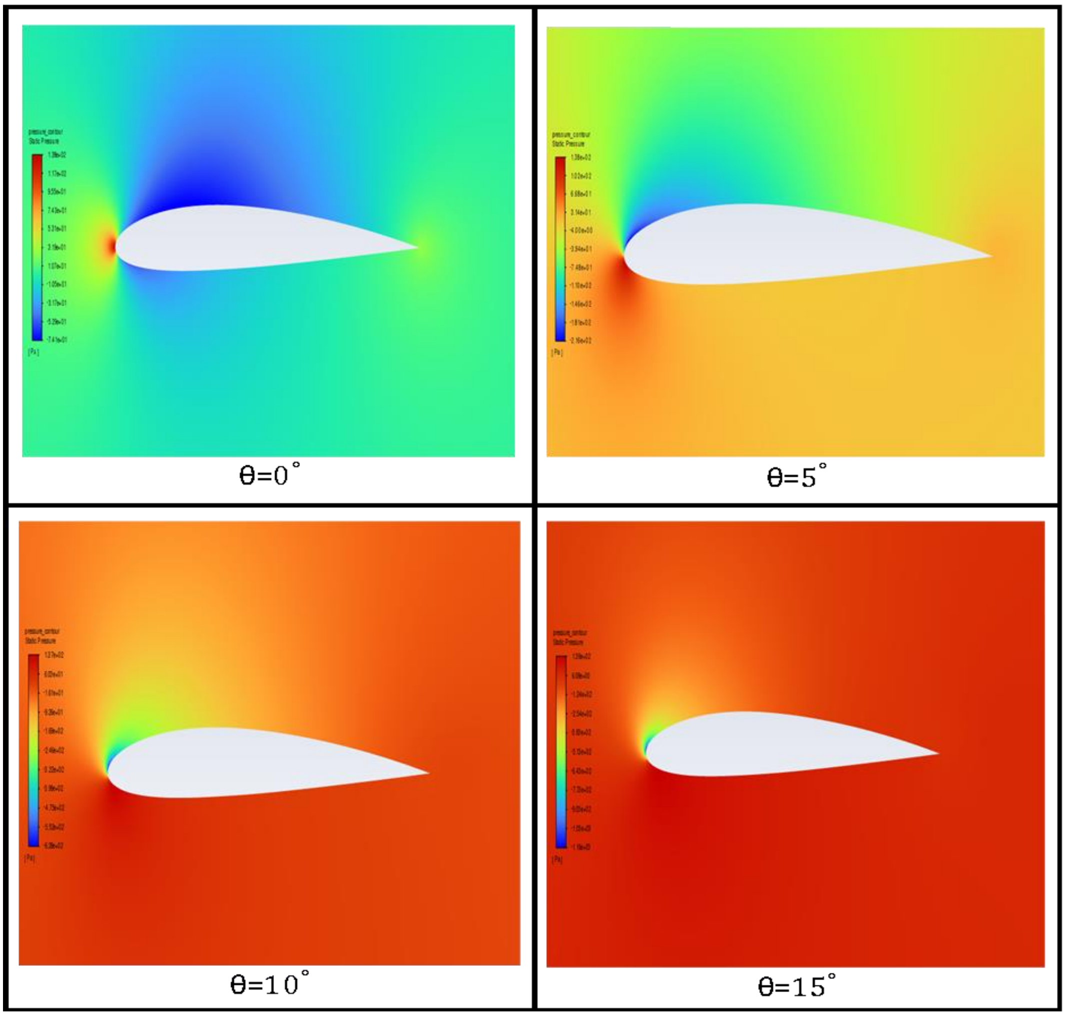

Fig 23: pressure contours 15m/s

The images show the pressure distribution around the airfoil at a velocity of 15 m/s and angles of attack of 0°, 5°, 10°, and 15°. At an angle of attack of 0°

the pressure distribution is nearly balanced between the upper and lower surfaces, with a slight pressure reduction over the upper surface, resulting in limited lift generation. As the angle of attack increases to 5°, the pressure on the upper surface decreases further while the pressure on the lower surface increases, leading to a noticeable increase in lift force. At 10°, the pressure difference becomes larger, with a wider low-pressure region appearing above the airfoil, indicating a significant increase in lift and improved aerodynamic performance. At an angle of attack of 15°, the greatest pressure difference between the upper and lower surfaces is observed, along with a clear expansion of the low-pressure region over the airfoil. This indicates the highest lift generation; however, it may also be accompanied by the onset of airflow disturbance and the approach of flow separation (stall).

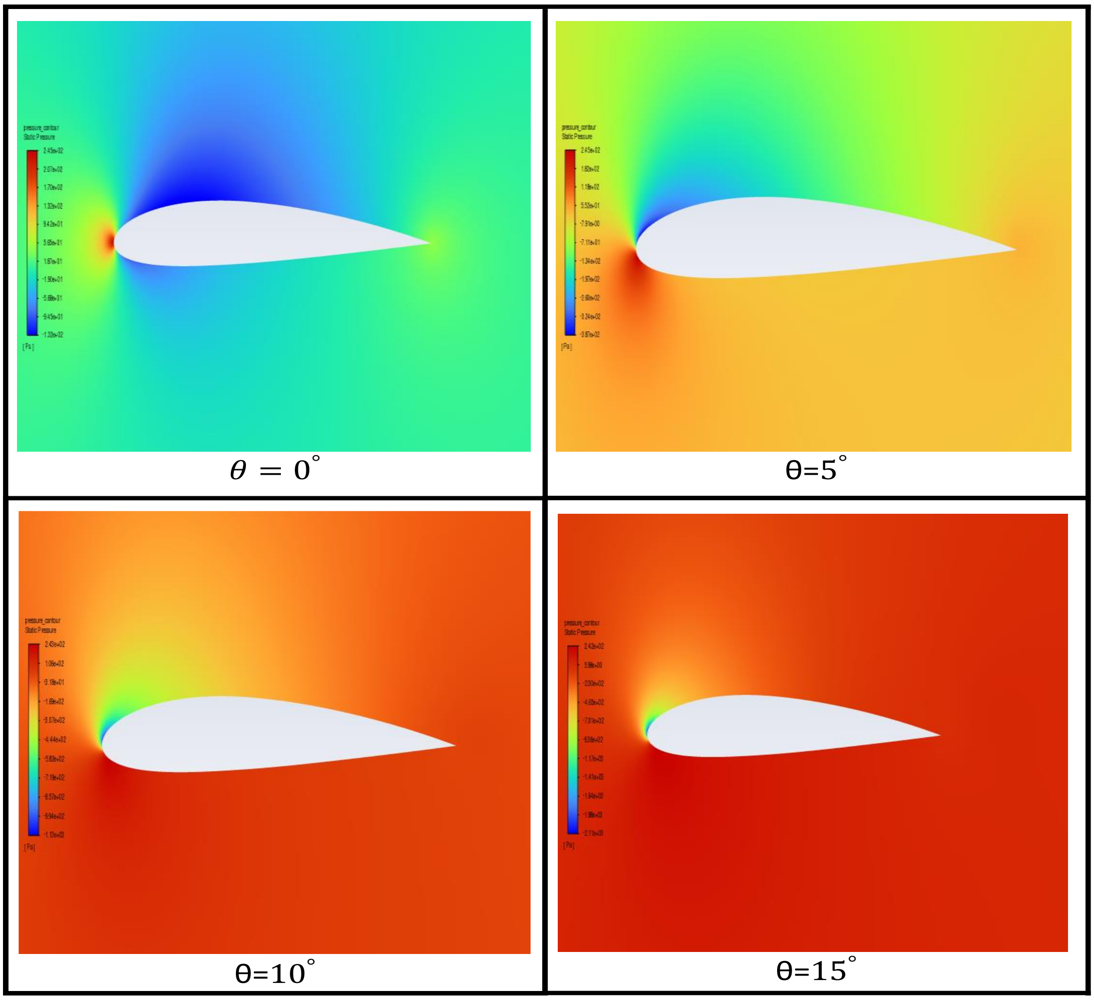

Fig 24: Pressure contours $20 m/s$

Fig 24: pressure contours 20 m/s

The images show the pressure distribution around the airfoil at a velocity of 20 m/s and angles of attack of 0°, 5°, 10°, and 15°. At an angle of attack of 0°, the pressure distribution is relatively balanced between the upper and lower surfaces, with a slight pressure decrease over the upper surface, resulting in a small lift force. As the angle of attack increases to 5°, the pressure reduction on the upper surface becomes more noticeable, while the pressure on the lower surface increases, leading to a higher lift force compared to the initial case. At an angle of attack of 10°, the pressure difference becomes greater, with a wide low-pressure region forming above the airfoil, indicating improved aerodynamic performance and a significant increase in lift force. At 15°, the largest pressure difference between the two surfaces is observed, along with a clear extension of the low-pressure region over the upper surface. This indicates the maximum lift generation at this velocity, although it may also be associated with the onset of airflow disturbance and the approach of flow separation (stall).

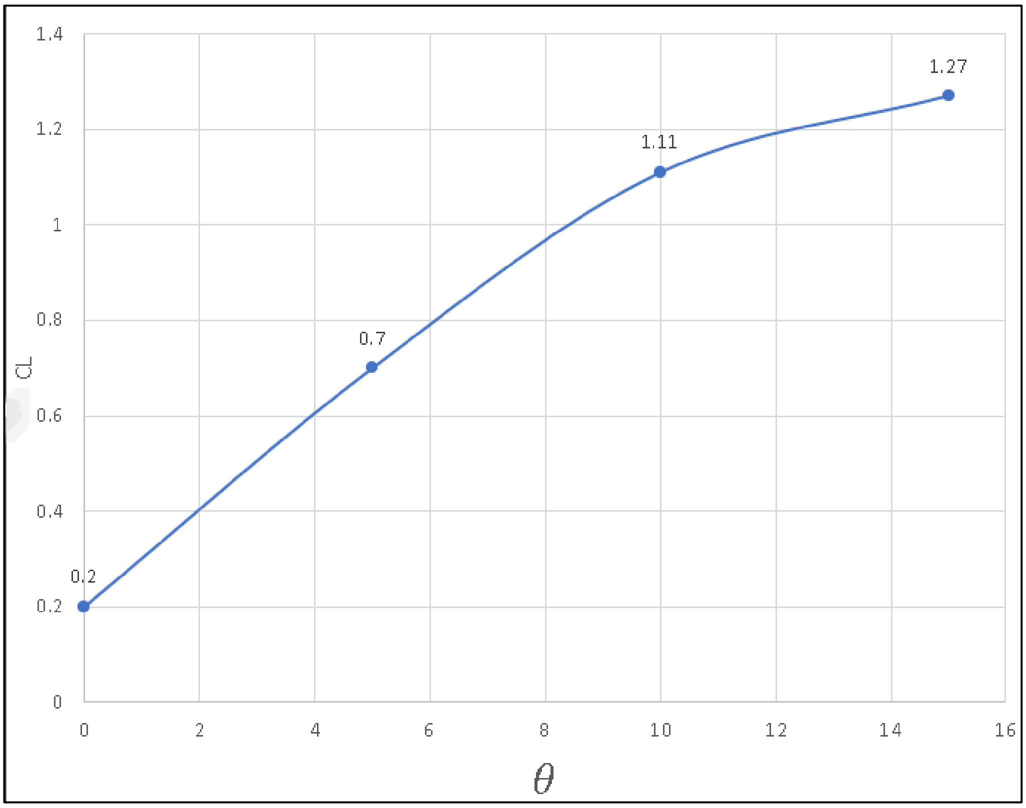

Fig 25: Variation of Lift Coefficient (CL) with Angle of Attack at 10 m/s

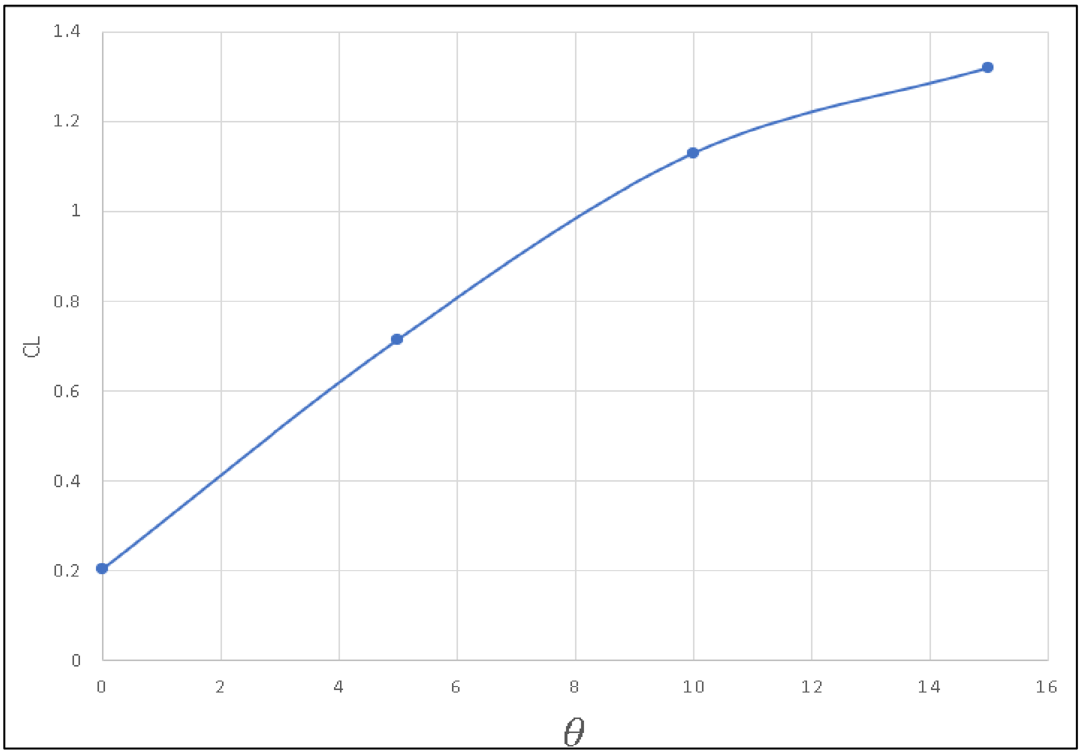

Fig 26: Variation of Lift Coefficient (CL) with Angle of Attack at 15 m/s

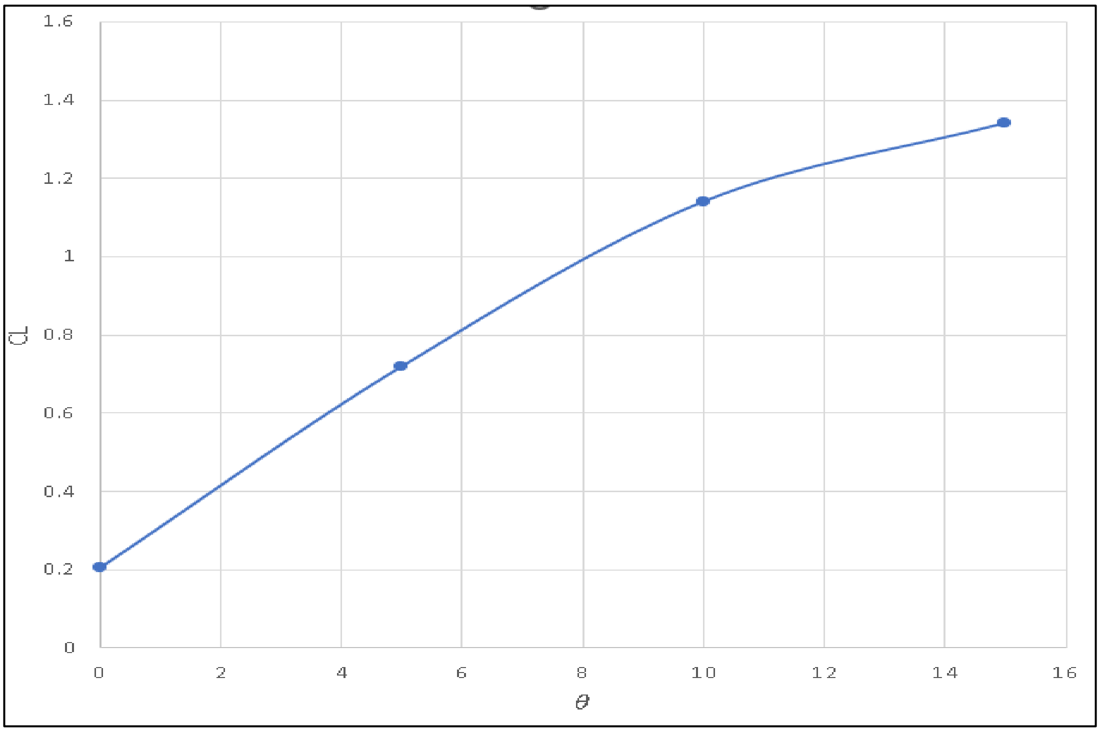

Fig 27: Variation of Lift Coefficient (CL) with Angle of Attack at 20 m/s

Commentary on the curves:

The lift coefficient (**CL**) curves show a continuous increase with the angle of attack from **0° to 15°** for all investigated velocities (**10, 15, and 20 m/s**). At an angle of attack of **0°**, the **CL** value is approximately **0.20** for all cases, then increases progressively as the angle of attack increases, reaching its maximum value at **15°**.

For the velocities of **10 m/s** and **15 m/s**, the **CL** values remain very close, reaching approximately **1.27** and **1.32**, respectively, at **15°**. At **20 m/s**, a slightly higher lift coefficient is observed, reaching about **1.34** at the same angle.

Furthermore, the rate of increase in **CL** is more pronounced between **0° and 10°**, while a gradual reduction in the growth rate is noticed between **10° and 15°**, indicating the onset of reduced lift enhancement at higher angles of attack.

Overall, the results demonstrate that increasing the angle of attack significantly improves the lift coefficient, whereas the effect of velocity is relatively limited within the studied range. The best aerodynamic performance is achieved at **20 m/s** and an angle of attack of **15°**.

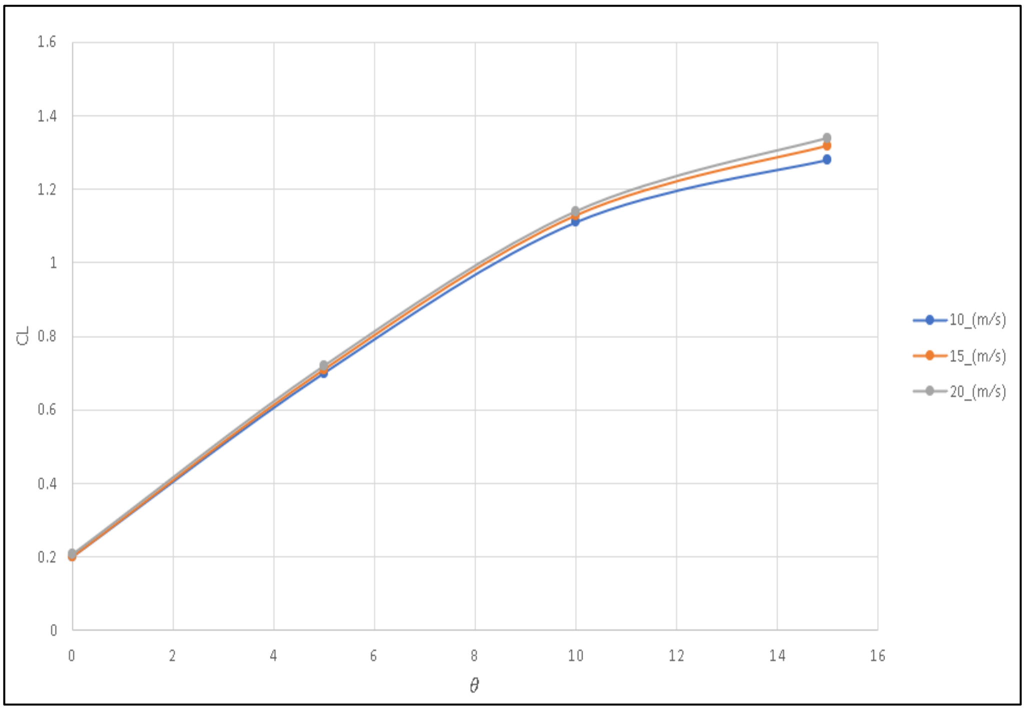

Fig 28: Variation of Lift Coefficient (CL) with Angle of Attack at Different Flow Velocities (10, 15, and 20 m/s)

Comparison:

A comparison of the lift coefficient (**CL**) curves at flow velocities of **10, 15, and 20 m/s** reveals a similar aerodynamic behavior for all cases. The lift coefficient increases steadily with the angle of attack from **0° to 15°**, indicating a direct relationship between these two parameters.

At low angles of attack, the **CL** values are nearly identical for all velocities, while slight differences become noticeable as the angle increases. The highest lift coefficient is achieved at **20 m/s**, followed by **15 m/s** and **10 m/s**, particularly at an angle of attack of **15°**, where the **CL** values reach approximately **1.34**, **1.32**, and **1.27**, respectively.

These results suggest that the angle of attack plays a more significant role in enhancing lift than the flow velocity within the investigated range. Nevertheless, increasing the velocity contributes to a moderate improvement in lift performance, with the best aerodynamic efficiency obtained at **20 m/s** and **15°** angle of attack.

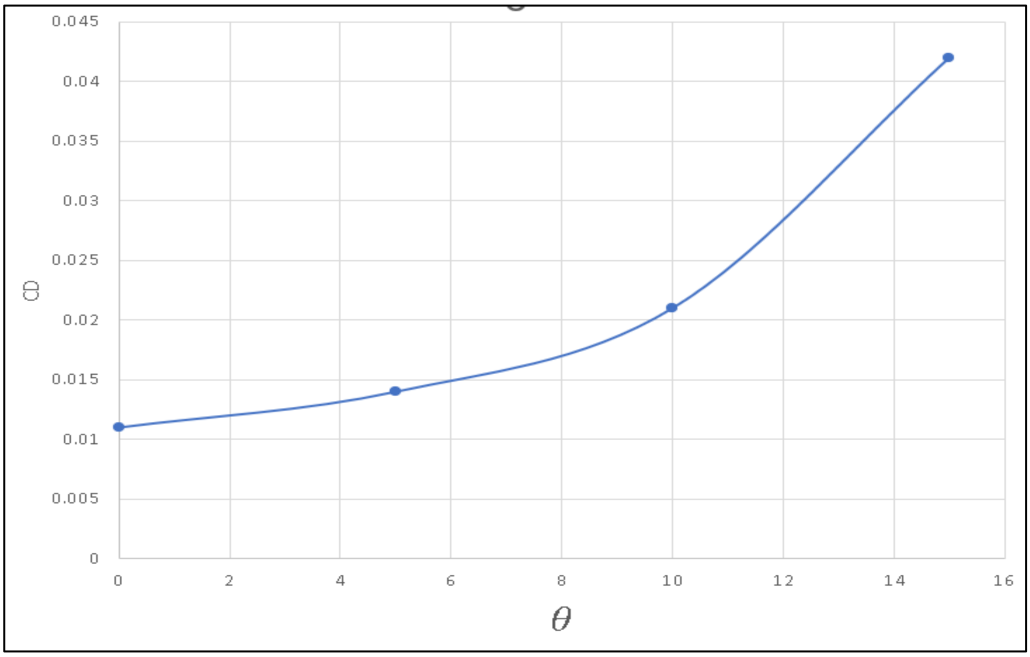

Fig 29: Variation of Drag Coefficient (CD) with Angle of Attack at 10 m/s

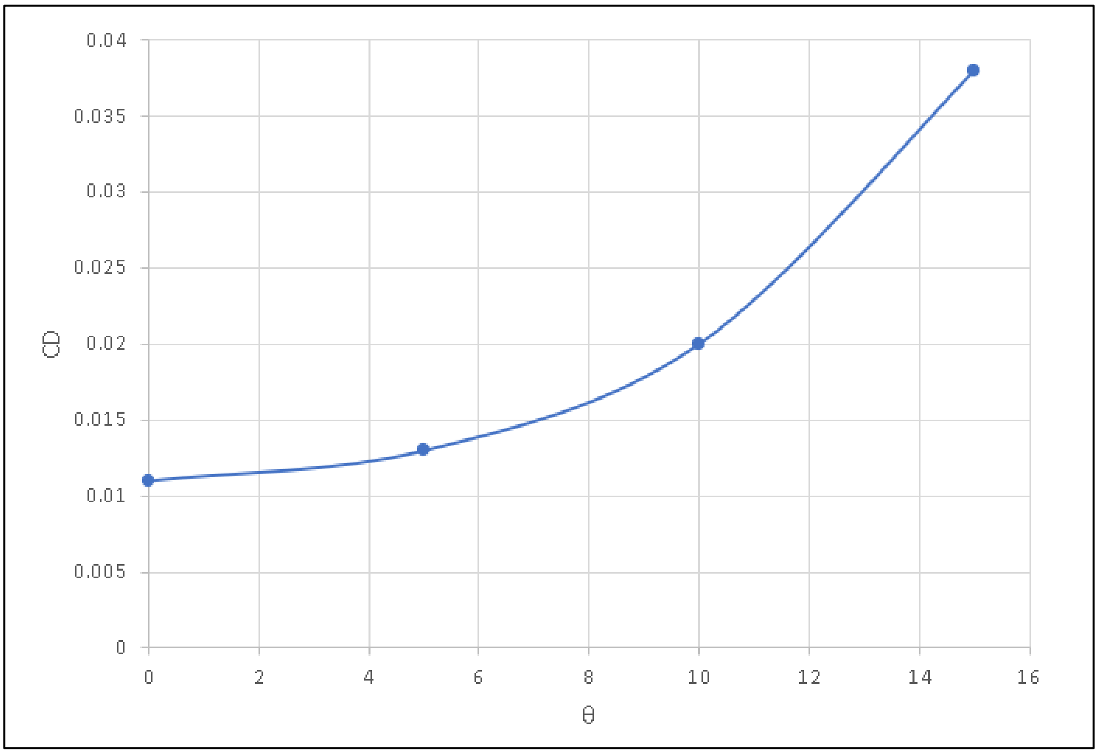

Fig 30: Variation of Drag Coefficient (CD) with Angle of Attack at 15 m/s

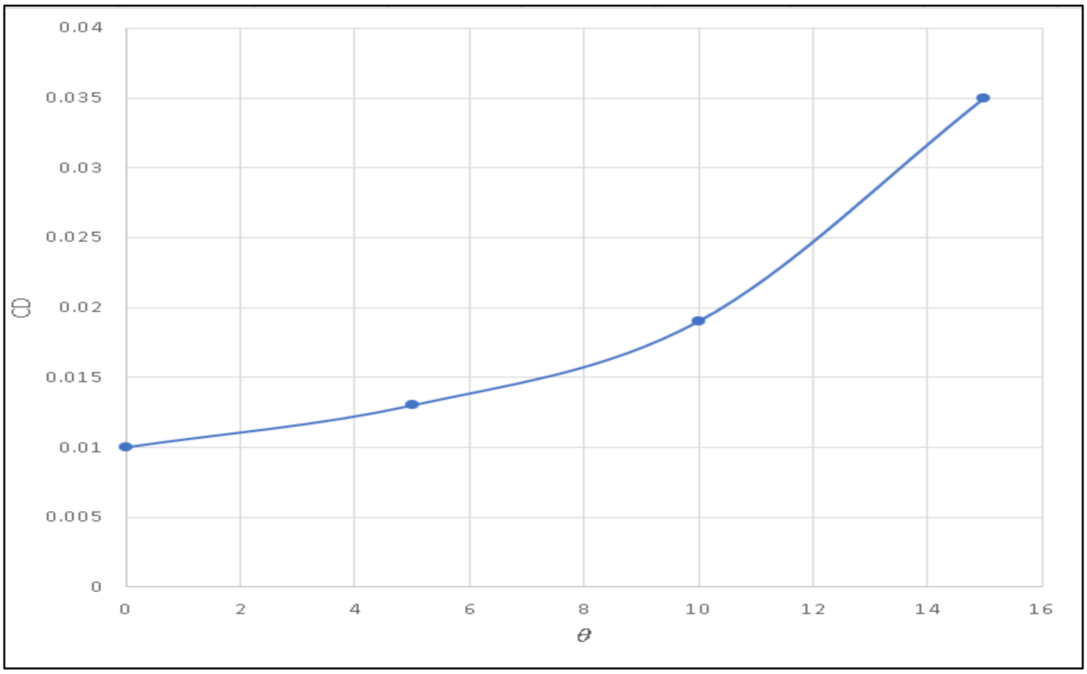

Fig 31: Variation of Drag Coefficient (CD) with Angle of Attack at 20 m/s

Commentary on the curves:

The obtained curves show that the drag coefficient (**CD**) increases continuously with the angle of attack, from **0° to 15°**, for all investigated velocities. The increase is relatively small between **0° and 5°**, becomes more noticeable at **10°**, and rises sharply at **15°**.

This behavior can be attributed to the increase in pressure differences around the airfoil and the growth of the boundary layer as the angle of attack increases, resulting in higher aerodynamic drag.

The results also indicate that the airflow remains relatively stable at low and moderate angles of attack, whereas flow separation effects become more significant at higher angles. This explains the rapid increase in drag coefficient values at **15°**.

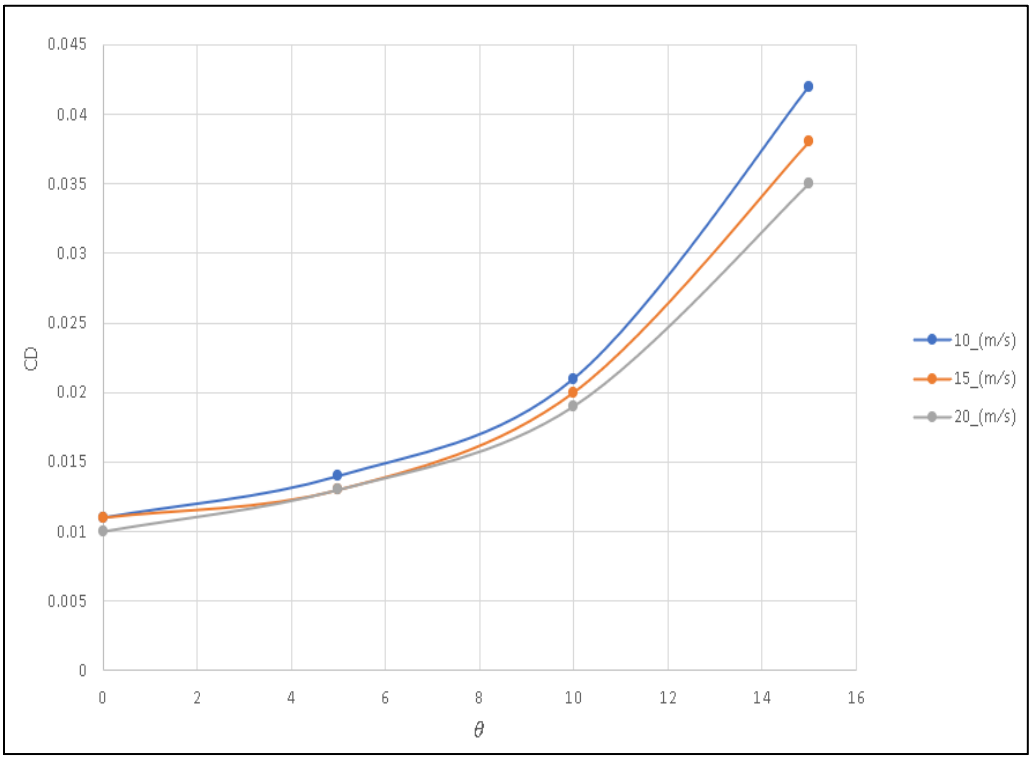

Fig 32: Variation of Drag Coefficient (CD) with Angle of Attack at Different Flow Velocities (10, 15, and 20 m/s)

Comparison:

A comparison of the three velocities (**10, 15, and 20 m/s**) reveals a similar overall trend, with the drag coefficient (**CD**) increasing as the angle of attack increases in all cases. However, the magnitude of **CD** differs from one velocity to another. The highest drag values are observed at **10 m/s**, particularly at an angle of attack of **15°**, while lower values are recorded at **15 m/s** and **20 m/s**. At **15°**, the drag coefficient reaches approximately **0.042** for **10 m/s**, **0.038** for **15 m/s**, and **0.035** for **20 m/s**. These results suggest that increasing the velocity within the investigated range improves the aerodynamic performance of the airfoil by reducing the drag coefficient. Nevertheless, the angle of attack remains the dominant parameter influencing the variation of **CD** throughout the study.

General conclusion

Conclusion

This study investigated the aerodynamic performance of airfoils using Computational Fluid Dynamics (CFD) in order to understand the main parameters governing airflow behavior and aerodynamic efficiency. The results showed that airfoil geometry, angle of attack, and flow velocity strongly influence lift and drag characteristics. Increasing the angle of attack increases lift due to a higher-pressure difference between the upper and lower surfaces, but it also increases drag because of stronger viscous effects and the onset of flow separation at higher angles.

The study demonstrated that optimal aerodynamic performance is achieved at low to moderate angles of attack, where the flow remains stable and attached, ensuring a good balance between lift and drag. At higher angles of attack, flow separation becomes more significant, leading to reduced efficiency and possible stall conditions.

The results also confirmed that NACA airfoils are well-suited for aerodynamic applications due to their efficient geometric design and stable performance over a wide range of conditions. In addition, the SST k–ω turbulence model proved to be reliable in predicting turbulent flow behaviour, particularly in regions with adverse pressure gradients and flow separation. Overall, CFD proved to be an effective and efficient tool for aerodynamic analysis, offering a practical alternative to experimental methods while providing detailed flow information. The study also highlights the importance of improving airfoil design to enhance aircraft performance and reduce fuel consumption.

Future work may focus on more advanced airfoil geometries, higher Reynolds number flows, improved turbulence modeling such as LES and DNS, and three dimensional aerodynemic effects including wingtip vortices and winglets.

References

References

[1] Nikolaou, E., Kilimtzidis, S., and Kostopoulos, V., "Winglet Design for Aerodynamic and Performance Optimization of UAVs via Surrogate Modeling," Aerospace, vol. 12, no. 1, p. 36, 2025.

[2] Panagiotou, P., Kaparos, P., and Yakinthos, K., "Winglet Design and Optimization for a MALE UAV Using CFD," Aerospace Science and Technology, vol. 39, pp. 190–205, 2014.

[3] Dela Peña, A., "A CFD-Based Comparative Analysis of Passive and Active Winglets for Narrow-Body Aircraft: Aerodynamic Performance, Fuel Efficiency, and Structural Trade-Offs," International Journal of Latest Technology in Engineering Management & Applied Science, vol. 14, no. 5, p. 10.51583, 2025.

[4] Lakhdhar, L., Bouabidi, A., and Snoussi, A., "Optimization of Aerodynamic Performances of UAV Propellers by the Integration of Winglets: Experimental Study and CFD Simulation," Aerospace Science and Technology, 2026, p. 112069.

[5] Belferhat, S., et al., "Aerodynamic Optimization of a Winglet Design," EPJ Web of Conferences, EDP Sciences, 2013.

[6] Sogukpinar, H., "Numerical Investigation of Influence of Diverse Winglet Configuration on Induced Drag," Iranian Journal of Science and Technology, Transactions of Mechanical Engineering, vol. 44, no. 1, pp. 203–215, 2020.

[7] Merryisha, S., and Rajendran, P., "Review of Winglets on Tip Vortex, Drag and Airfoil Geometry," Journal of Advanced Research in Fluid Mechanics and Thermal Sciences, vol. 63, no. 2, pp. 218–237, 2019.

[8] Reddy, S.R., et al., "Multi-Winglets: Multi-Objective Optimization of Aerodynamic Shapes," Proceedings of the 53rd AIAA Aerospace Sciences Meeting, 2015.

[9] Helal, H., et al., "Aerodynamic Analyses of Aircraft-Blended Winglet Performance," IOSR Journal of Mechanical and Civil Engineering, vol. 13, no. 3, pp. 2320–334, 2016.

[10] Bachmann, C.D., Experimental and Numerical Investigation of NACA Airfoil Wing with Winglets, 2021.

[11] Al-Khafaji, A.J.D., Panatov, G.S., and Boldyrev, A.S., "Numerical Analysis and Optimization of a Winglet Sweep Angle and Winglet Tip Chord for Improvement of Aircraft Flight Performance," Diagnostyka, vol. 23, 2022.

[12] Madani, S.A.S., Vaezi, E., and Keshmiri, A., "CFD-Driven Evaluation of Winglet Cant Angle: Insights into Aerodynamic and Aeroacoustic Performance," Results in Engineering, vol. 26, p. 104759, 2025.

[13] Babu, D.P.R., et al., "Evaluation of Traditional and Slotted Winglets for Enhanced Aerodynamic Efficiency," Physics of Fluids, vol. 37, no. 2, 2025.

[14] Gray, A.L., and Zingg, D.W., "Blended-Wing-Body Regional Aircraft Optimization with High-Fidelity Aerodynamics and Critical Design Requirements," Journal of Aircraft, vol. 61, no. 6, pp. 1775–1792, 2024.

[15] Gibbs-Smith, C.H., The Invention of the Aeroplane 1799–1909, Faber and Faber, London, 1966.

[16] Hallion, A.R., Taking Flight: Inventing the Aerial Age, from Antiquity through the First World War, Oxford University Press, 2003.

[17] Jacobs, E.N., Ward, K.E., and Pinkerton, R.M., The Characteristics of 78 Related Airfoil Sections from Tests in the Variable-Density Wind Tunnel, NACA Report No. 460, National Advisory Committee for Aeronautics, 1933.

[18] Abbott, I.H., and Von Doenhoff, A.E., Theory of Wing Sections: Including a Summary of Airfoil Data, Dover Publications, New York, 1959.

[19] Lyu, Z., and Martins, J.R., "RANS-Based Aerodynamic Shape Optimization of a Blended-Wing-Body Aircraft," Proceedings of the 21st AIAA Computational Fluid Dynamics Conference, 2013.

[20] Evolution of an Airfoil. Available: https://vintageaviationnews.com/warbird-articles/evolution-of-an-airfoil.html

[21] Design, Fabrication and Numerical Analysis on NACA 642-215, 2015.

[22] Stephen, C., Introduction to Aerospace Engineering with a Flight Test Perspective, John Wiley & Sons Ltd, United Kingdom, 2017.

[23] N.F.-D. Series, "The NACA Airfoil Series," 2012.

[24] Clark Y Airfoil. Available: https://en.wikipedia.org/wiki/Clark_Y_airfoil

[25] Royal Air Force, "Our History," RAF Official Website. Available: https://www.raf.mod.uk/what-we-do/our-history/ (Accessed: May 20, 2026).

[26] Airfoil Geometries. Available: https://eaglepubs.erau.edu/introductiontoaerospaceflightvehicles/chapter/airfoil-geometries/

[27] Imumbhon, J.O., Alam, M.D., and Cao, Y., 2021.

[28] Whitcomb, R.T., "A Design Approach and Selected Wind-Tunnel Results at High Subsonic Speeds for the Supercritical Wing," NASA Technical Report, National Aeronautics and Space Administration, 1976.

[29] Babu, D.P.R., et al., "Evaluation of Traditional and Slotted Winglets for Enhanced Aerodynamic Efficiency," Physics of Fluids, vol. 37, no. 2, 2025.

[30] Cours Aérodynamique et Mécanique du Vol (Tome II), Équipe Aéronautique France.

[31] Houghton, E.L., and Carpenter, P.W., Aerodynamics for Engineering Students, London, 2003.

[32] Stephen, C., Introduction to Aerospace Engineering with a Flight Test Perspective, John Wiley & Sons Ltd, United Kingdom, 2017.

[33] Wilcox, D.C., Turbulence Modeling for CFD, DCW Industries, 1998.

[34] Tu, J., Yeoh, G.H., and Liu, C., Computational Fluid Dynamics: A Practical Approach, Elsevier, 2008.

[35] Blazek, J., Computational Fluid Dynamics: Principles and Applications, Elsevier Science Ltd, 2001.

[36] Babu, D.P.R., et al., "Evaluation of Traditional and Slotted Winglets for Enhanced Aerodynamic Efficiency," Physics of Fluids, vol. 37, no. 2, 2025.

[37] Hirsch, C., Numerical Computation of Internal and External Flows, John Wiley & Sons, 2007.

[38] Lallemand, A., Dynamique des Fluides Réels, Techniques de l'Ingénieur, 1981.

[39] Menter, F.R., "Two-Equation Eddy-Viscosity Turbulence Models for Engineering Applications," AIAA Journal, vol. 32, pp. 1598–1605, 1994.

[40] Boukhemla, B., and Douaissia, O., "Simulation Numérique de l'Écoulement Autour d'un Profil Oscillant," Projet de Fin d'Étude, 2008/2009.

[41] Tulapurkara, E.G., "Turbulence Models for Computation of Flow Past Airplanes," Progress in Aerospace Sciences, vol. 33, pp. 71–165, 1997.

[42] V., F., Étude Expérimentale et Numérique du Contrôle Actif de Jets dans des Chambres de Combustion, Thèse de Doctorat, Institut National Polytechnique de Toulouse, 2003.

[43] Design and Structural Analyses of a Reciprocating S1223 High-Lift Wing for an RA-Driven VTOL UAV, Aerospace, vol. 8, no. 8, p. 214, MDPI, 2021.